Electrocatalytic Oxidation by Binuclear Ruthenium Complexes Incorporating the Anionic Tripod Ligand $[(\eta^5\text{-}C_5H_5)Co\{(CH_3O)_2P{=}O\}_3]^-$ †

Eric P. Kelson, Lawrence M. Henling, William P. Schaefer, Jay A. Labinger,* and John E. Bercaw*

Arnold and Mabel Beckman Laboratories of Chemical Synthesis and the Beckman Institute, California Institute of Technology, Pasadena, California 91125

Received December 16, 1992

The two-phase reaction of NaL_{OMe} (L_{OMe} = $[(\eta^5\text{-}C_5H_5)Co\{P(O)(OCH_3)_2\}_3]^-$) in 1% H_2SO_4 with RuO_4 in CCl_4 affords the edge-sharing octahedral dimer $[(L_{OMe})(HO)Ru^{IV}(\mu\text{-}O)_2Ru^{IV}(OH)(L_{OMe})]$ which is diprotonated by aqueous CF_3SO_3H to the corresponding salt $[(L_{OMe})(H_2O)Ru^{IV}(\mu\text{-}O)_2Ru^{IV}(OH_2)(L_{OMe})][CF_3SO_3]_2$. This dimer salt is oxidized by C_6H_5IO in CH_3CN to $[(L_{OMe})(O)Ru^{V}(\mu\text{-}O)_2Ru^{V}(O)(L_{OMe})]$ and reduced by alcohols, aldehydes, or triphenylphosphine in CH_3CN to $[(L_{OMe})(CH_3CN)Ru^{III}(\mu\text{-}OH)_2Ru^{III}(NCCH_3)(L_{OMe})][CF_3SO_3]_2$. In buffered aqueous solution, the diprotonated Ru^{IV}–Ru^{IV} dimer reacts with formaldehyde to afford a triply bridged dimer, $[(L_{OMe})Ru^{III}(\mu\text{-}OH)_2(\mu\text{-}HCOO)Ru^{III}(L_{OMe})][CF_3SO_3]$. The latter reaction appears to be autocatalytic via an inner-sphere mechanism. The Ru^{III}–Ru^{III} formate adduct is oxidized by $AgCF_3SO_3$ to the Ru^{IV}–Ru^{IV} analog $[(L_{OMe})Ru^{IV}(\mu\text{-}O)_2(\mu\text{-}HCOO)Ru^{IV}(L_{OMe})][CF_3SO_3]$, which slowly reacts with aqueous formaldehyde to regenerate the Ru^{III}–Ru^{III} adduct and free formate. The dimeric system in aqueous solution functions as an electrocatalyst for the oxidation of formaldehyde at low anodic potentials (near 0.0 V versus SCE at pH 8.5). Both Ru^{III}–Ru^{III} dimers have been characterized by X-ray crystallography. Crystal data: $[(L_{OMe})(CH_3CN)Ru^{III}(\mu\text{-}OH)_2Ru^{III}(NCCH_3)(L_{OMe})][CF_3SO_3]_2$, $Ru_2Co_2C_{28}H_{54}O_{26}N_2P_6S_2F_6$, triclinic, $P\bar{1}$, with a = 8.626(3) Å, b = 12.275(2) Å, c = 13.457(3) Å, α = 71.32(2)°, β = 85.35(2)°, γ = 80.01(3)°, V = 1328.9(6) Å^3, Z = 2, $R(F_o)$ = 0.040; $[(L_{OMe})Ru^{III}(\mu\text{-}OH)_2(\mu\text{-}HCOO)Ru^{III}(L_{OMe})][CF_3SO_3]\cdot 2H_2O$, $Ru_2Co_2C_{24}H_{53}O_{27}P_6SF_3$, monoclinic, $P2_1/n$, with a = 14.356(2) Å, b = 23.839(6) Å, c = 15.284(3) Å, β = 115.44(1)°, V = 4723.5(18) Å^3, Z = 4, $R(F_o)$ = 0.033.

Introduction

Much research has been published concerning the design and synthesis of metal complexes as catalysts for the oxidation of organic substrates. Mechanisms invoking oxo transfer, electron transfer, and hydrogen and hydride transfer have been proposed for oxidations by OsO_4,[1] metalloporphyrins,[2] and other metal oxo complexes. Ruthenium complexes have attracted particular interest, due in part to the wide range of accessible oxidation states. Most of these complexes are monomeric and operate via higher oxidation states Ru(V),[3,4] Ru(VI),[5,6] or Ru(VII).[7] A number of complexes are known which use the lower states Ru(IV)[4,6,8,9] and Ru(III).[4,8] Like those of the higher oxidation states, these complexes are strong oxidizing agents.

One attractive application of such complexes is as electrocatalysts in fuel cells that can operate directly on organic fuels such as methanol or formaldehyde. Such fuel cells exhibit current–voltage properties much poorer than those of standard H_2–O_2 fuel cells due to slower oxidation of the organic fuel and electrode poisoning by oxidation intermediates and products such as CO.

† Contribution No. 8778.

(1) Jacobsen, E. N.; Markó, I.; France, M. B.; Svendsen, J. S.; Sharpless, K. B. *J. Am. Chem. Soc.* **1989**, *111*, 737–739. Wai, J. S. M.; Markó, I.; Svendsen, J. S.; Finn, M. G.; Jacobsen, E. N.; Sharpless, K. B. *J. Am. Chem. Soc.* **1989**, *111*, 1123–1125. Ogino, Y.; Chen, H.; Kwong, H.-L.; Sharpless, K. B. *Tetrahedron Lett.* **1991**, *32*, 3965–3968.

(2) Groves, J. T.; Stern, M. K. *J. Am. Chem. Soc.* **1987**, *109*, 3812–3814. Traylor, T. G.; Xu, F. *J. Am. Chem. Soc.* **1988**, *110*, 1953-1958. Groves, J. T.; Stern, M. K. *J. Am. Chem. Soc.* **1988**, *110*, 8628–8638. Traylor, T. G.; Miksztal, A. R. *J. Am. Chem. Soc.* **1989**, *111*, 7443–7448. Groves, J. T.; Viski, P. *J. Am. Chem. Soc.* **1989**, *111*, 8537–8538. Traylor, T. G. *Pure Appl. Chem.* **1991**, *63*, 265–274.

(3) Che, C.-M.; Yam, V. W.-W. *J. Am. Chem. Soc.* **1987**, *109*, 1262. Wong, K.-Y.; Che, C.-M.; Anson, F. C. *Inorg. Chem.* **1987**, *26*, 737. Raven, S. J.; Meyer, T. J. *Inorg. Chem.* **1988**, *27*, 4478–4483. Denggel, A. C.; Griffith, W. P.; O'Mahoney, C. A.; Williams, D. J. *J. Chem. Soc.*, **1989**, 1720. Che, C.-M.; Yam, V. W.-W.; Mak, T. C. *J. Am. Chem. Soc.* **1990**, *112*, 2284. Che, C.-M.; Ho, C.; Lau, T. C. *J. Chem. Soc., Dalton Trans.* **1991**, 1259. Che, C.-M.; Ho, C.; Lai, T.-C. *J. Chem. Soc., Dalton Trans.* **1991**, 1910.

(4) Llobet, A.; Hodgson, D. J.; Meyer, T. J. *Inorg. Chem* **1990**, *29*, 3760–3766.

(5) Che, C.-M.; Leung, W.-H.; Poon, C.-K. *J. Chem. Soc., Chem. Commun.* **1987**, 173. Bailey, C. L.; Drago, R. S. *J. Chem. Soc., Chem. Commun.* **1987**, 179. Che, C.-M.; Leung, W. H. *J. Chem. Soc., Chem. Commun.* **1987**, 1376. Che, C.-M.; Lee, W.-O. *J. Chem. Soc., Chem. Commun.* **1988**, 881. Lau, T.-C.; Che, C.-M.; Lee, W.-O.; Poon, C.-K. *J. Chem. Soc., Chem. Commun.* **1988**, 1406. El-Hendawy, A. M.; Griffith, W. P.; Taha, F. I.; Moussa, M. N. *J. Chem. Soc., Dalton Trans.* **1989**, 901. Che, C.-M.; Tang, W.-T.; Lee, W.-O.; Wong, W.-T.; Lai, T.-F. *J. Chem. Soc., Dalton Trans.* **1989**, 2011. Che, C.-M.; Wong, K.-Y. *J. Chem. Soc., Dalton Trans.* **1989**, 2065. Che, C.-M.; Tang, W.-T.; Wong, W.-T.; Lai, T.-F. *J. Am. Chem. Soc.* **1989**, *111*, 9048. Griffith, W. P.; Jolliffe, J. M.; Ley, S. V.; Willimas, D. J. *J. Chem. Soc., Chem. Commun.* **1990**, 1219. Dovletoglou, A.; Adeyemi, S. A.; Lynn, M. H.; Hodgeson, D. J.; Meyer, T. J. *J. Am. Chem. Soc.* **1990**, *112*, 8989–8990. Goldstein, A. S.; Drago, R. S. *J. Chem. Soc., Chem. Commun.* **1991**, 21. Che, C.-M.; Leung, W.-H.; Li, C.-K.; Poon, C.-K. *J. Chem. Soc., Dalton Trans.* **1991**, 379.

(6) Groves, J. T.; Quinn, R. *Inorg. Chem.* **1984**, *23*, 3844–3846. Groves, J. T.; Quinn, R. *J. Am. Chem. Soc.* **1985**, *107*, 5790. Llobet, A.; Groves, J. T.; Ahn, K.-H. *Inorg. Chem.* **1987**, *26*, 3831–3832. Leung, W.-H.; Che, C. M. *J. Am. Chem. Soc.* **1989**, *111*, 8812.

(7) Green, G.; Griffith, W. P.; Hollinshead, D. M.; Ley, S. V.; Schröder, M. *J. Chem. Soc., Perkin Trans.* **1984**, 681. Griffith, W. P.; Ley, S. V.; Whitcombe, G. P.; White, A. D. *J. Chem. Soc., Chem. Commun.* **1987**, 1625.

(8) Samuels, G. J.; Meyer, T. J. *J. Am. Chem. Soc.* **1981**, 307–312. Meyer, B. A.; Sipe, B. K.; Meyer, T. J. *Inorg. Chem.* **1981**, *20*, 1475–1480. Binstead, R. A.; Moyer, B. A.; Samuels, G. J.; Meyer, T. J. *J. Am. Chem. Soc.* **1981**, *103*, 2897–2899. Thompson, M. S.; Meyer, T. J. *J. Am. Chem. Soc.* **1982**, *104*, 4106–4115. Thompson, M. S.; Meyer, T. J. *J. Am. Chem. Soc.* **1982**, *104*, 5070–5076. Thompson, M. S.; De Giovani, W. F.; Moyer, B. A.; Meyer, T. J. *J. Org. Chem.* **1984**, *49*, 4972–4977. Dobson, J. C.; Seok, W. K.; Meyer, T. J. *Inorg. Chem.* **1986**, *25*, 1513–1514. Roecker, L.; Meyer, T. J. *J. Am. Chem. Soc.* **1986**, *108*, 4066–4073. Roecker, L.; Meyer, T. J. *J. Am. Chem. Soc.* **1987**, *109*, 746–754. Roecker, L.; Dobson, J. C.; Vining, W. J.; Meyer, T. J. *Inorg. Chem.* **1987**, *26*, 779–781. Seok, W. K.; Dobson, J. C.; Meyer, T. J. *Inorg. Chem.* **1988**, *27*, 3–5.

(9) Marmion, M. E.; Takauchi, K. J. *J. Am. Chem. Soc.* **1986**, *108*, 510. Marmion, M. E.; Takeuchi, K. J. *J. Chem. Soc., Chem. Commun.* **1987**, 1396. Leising, R. A.; Takeuchi, K. J. *Inorg. Chem.* **1987**, 4391. Marmion, M. E.; Takeuchi, K. J. *J. Chem. Soc., Dalton Trans.* **1988**, 2385. Ho, C.; Che, C.-M.; Lau, T.-C. *J. Chem. Soc., Dalton Trans.* **1990**, 967. Che, C.-M.; Ho, C.; Lau, T.-C. *J. Chem. Soc., Dalton Trans.* **1991**, 1901.

0020-1669/93/1332-2863$04.00/0

Incorporation of a metal complex oxidation catalyst into the electrode could give substantial improvement. A number of known complexes are highly efficient for substrate oxidation, and molecular complexes are generally less susceptible to poisoning than heterogeneous surfaces. However, this scheme may still result in lower efficiency relative to H_2–O_2 fuel cells which operate at anodic potentials close to 0 V versus NHE. The minimum anodic potential of a cell with a molecular catalyst will be the redox potential of the catalyst: the higher this value, the lower the working voltage obtainable from the cell potentials. According to the consensus of the fuel cell industry, an anodic potential of no higher than 0.2 V versus NHE (0.0 V versus SCE) would be required for practical application.[10] Unfortunately, none of the catalysts mentioned above have potentials near this value.

We previously reported synthetic and structural studies on a dimeric ruthenium system[11] based upon the ligand $[(\eta^5\text{-}C_5H_5)\text{-}Co\{P(O)(OR)_2\}_3]^-$, originally reported by Kläui[12] and abbreviated as $(L_{OR})^-$. This system differs from other reported ruthenium catalysts, including dimers,[13] in that the metal centers have solely oxygen donor coordination environments. We have found that this system is capable of oxidizing organic substrates such as aldehydes via a redox couple whose potential is close to the required value. In this paper we report the chemical and electrochemical investigations of these oxidations and the characterization of several new complexes.

Experimental Section

General Considerations. NMR spectra were recorded on the Bruker AM500 (^{1}H, 500.1 MHz), Jeol JNM-GX400 (^{1}H, 399.65 MHz; ^{13}C, 100.40 MHz; ^{31}P, 161.70 MHz), and General Electric QE 300 (^{1}H, 300.10 MHz; ^{13}C, 75.47 MHz) Fourier transform spectrometers in D_2O (δ 4.63 ppm), CD_2Cl_2 (δ 5.32 ppm), $CDCl_3$ (δ 7.24 ppm), or CD_3CN (δ 1.93 ppm). UV–vis spectra were recorded on a Hewlett-Packard 8452A diode array spectrophotometer equipped with a Hewlett-Packard 89090A thermostated cell holder. The HP8452A was controlled from a IBM compatible Compaq Deskpro computer by Hewlett Packard software. Infrared spectra were recorded as Nujol mulls between KBr plates with a Perkin-Elmer 1600 Series FTIR. Elemental analyses for carbon, hydrogen, and nitrogen were carried out in the Caltech Analytical Laboratory by Fenton Harvey.

Most manipulations were carried out in air, except for syntheses of $Na(L_{OMe})$, $[(L_{OMe})(O)Ru^V(\mu\text{-}O)_2Ru^V(O)(L_{OMe})]$, $[(L_{OMe})(H_2O)Ru^{III}(\mu\text{-}OH)(\mu\text{-}OH_2)Ru^{III}(OH_2)(L_{OMe})](CF_3SO_3)_3$, and $[(L_{OMe})Ru^{III}(\mu\text{-}OH)_2(\mu\text{-}OH_2)Ru^{III}(L_{OMe})](CF_3SO_3)_2$ which were carried out under an inert atmosphere with vacuum-line techniques. Water was used as collected from a Barnstead nanopurifier train. Most of the organic solvents including petroleum ether, heptane, and toluene were obtained in the analytical grade and were used after drying with molecular sieves. CH_3CN and CD_3CN were further dried over CaH_2 and then distilled onto, refluxed over, and distilled from P_2O_5. $RuCl_3\cdot nH_2O$ (Aesar), $Co(acac)_2$ (sublimed) (Alfa), NaC_5H_5 (Aldrich), $HP(O)(OCH_3)_2$ (Aldrich), NaCN (Aldrich), CF_3SO_3H (Aldrich), $C_6H_5I(O_2CCH_3)_2$ (Aldrich), 40% $[N(CH_2CH_3)_4]^+(OH)^-$(aq) (Thiokol), $P(C_6H_5)_3$ (Aldrich), $OP(C_6H_5)_3$ (Aldrich), $P(CH_3)_3$ (Aldrich), 37% (w/w) CH_2O(aq) (Aldrich), 19% (w/w) $^{13}CH_2O$(aq) (CIL), and other reagents and solvents were used as obtained without further purification. The sodium salt $Na\{(\eta^5\text{-}C_5H_5)Co[P(O)(OCH_3)_2]_3\} = Na(L_{OMe})$, the RuO_4 solution in CCl_4, and C_6H_5IO were synthesized by published procedures.[14,15,16]

$(L_{OMe})(HO)Ru^{IV}(\mu\text{-}O)_2Ru^{IV}(OH)(L_{OMe})$ (1). This synthesis is analogous to that reported for $(L_{OEt})(HO)Ru^{IV}(\mu\text{-}O)_2Ru^{IV}(OH)(L_{OEt})$ by Power *et al.*[11] A CCl_4 solution of RuO_4 (86 mL of a 13 g L^{-1} solution, 7.0 mmol) was added dropwise to a solution of $Na(L_{OMe})$ (4.00 g, 8.44 mmol) in 1% H_2SO_4 (78 mL, 7.8 mmol) at 0 °C. During the addition, the solution changed from yellow to dark green-brown. The solution was stirred at 0 °C for 30 min and for a further 60 min as the solution warmed to room temperature. The dark aqueous layer was carefully separated from the organic layer and filtered through a medium frit to remove an intractable brown residue. A solution of Na_2CO_3 (3.39 g in 10 mL of H_2O, 32.0 mmol) was added, and the resulting suspension was allowed to settle for 5 min. The mixture of soluble green and insoluble brown solids was collected on a medium frit and then repeatedly resuspended in H_2O and refiltered until the filtrate was no longer green. The combined filtrates were extracted with CH_2Cl_2, and the organic solution dried with anhydrous $MgSO_4$ and filtered. Petroleum ether (1.5 times the volume of CH_2Cl_2) was added, and the settled precipitate was quickly isolated on a medium frit and washed with 2:3 (v/v) CH_2Cl_2/petroleum ether. The green solid was dried *in vacuo* (0.99 g, 0.85 mmol, 24% based on RuO_4). Anal. Calcd for $C_{22}H_{48}Co_2O_{22}P_6Ru_2$ (mol wt 1170.46): C, 22.58; H, 4.13. Found: C, 22.90; H, 4.02. IR (Nujol): 3646 (vw), 3599 (vw), 3452 (w), 3123 (vw), 1784 (vw), 1646 (vw), 1577 (vw), 1302 (vw), 1207 (vw), 1178 (w), 1075 (s), 1041 (s), 845 (s), 789 (s), 738 (s), 693 (vw), 600 (m), 558 (w). ^{1}H NMR (CD_3CN): δ 5.04 (s, C_5H_5, 10H), 3.86 (m, OCH_3, 12H), 3.66 (m, OCH_3, 12H), 3.52 (m, OCH_3, 12H), 2.21 (br s, OH). ^{1}H NMR (D_2O, pH = 7): δ 5.26 (s, C_5H_5, 10H), 3.89 (m, OCH_3, 12H), 3.66 (m, OCH_3, 12H), 3.57 (m, OCH_3, 12H). ^{1}H NMR (CD_2Cl_2): δ 5.11 (s, C_5H_3, 10H), 3.97 (t, J_{HP} = 5.7 Hz, OCH_3, 12H), 3.73 (t, J_{HP} = 5.7 Hz, OCH_3, 12H), 3.56 (s, J_{HP} = 11.4 Hz, OCH_3, 12H). UV–vis [λ_{max}, nm (ϵ, M^{-1} cm^{-1}), in pH = 7 H_2O]: 210 (2.7×10^4), 240 (4.1×10^4), 340 (1.26×10^4), 680 nm (2.0×10^3).

$[(L_{OMe})(H_2O)Ru^{IV}(\mu\text{-}O)_2Ru^{IV}(OH_2)(L_{OMe})](CF_3SO_3)_2$ ($[H_21](CF_3SO_3)_2$). An excess of concentrated CF_3SO_3H (1 mL, 11.3 mmol) was added dropwise to dimer **1** (0.99 g, 0.85 mmol) suspended in H_2O (22 mL). The suspension turned from yellowish-green to bluish-green. The solution was stirred at room temperature for 10 min and allowed to settle for 5 min. The solid was collected on a medium frit and washed repeatedly with aqueous CF_3SO_3H (1 mL in 22 mL H_2O) until the washings were colorless. The solid was then washed with H_2O (3 x 1 mL) and dried *in vacuo* (1.10 g. 0.75 mmol, 88%). Anal. Calcd for $C_{24}H_{50}Co_2F_6O_{28}P_6Ru_2S_2$ (mol wt 1470.60): C, 19.60; H, 3.43. Found: C, 19.56; H, 3.32. IR (Nujol): 3394 (br, vw), 3168 (br, w), 3118 (vw), 1805 (vw), 1631 (vw), 1564 (vw), 1296 (s), 1239 (m), 1225 (m), 1180 (w), 1170 (w), 1159 (w), 1147 (w), 1063 (sh, s), 1043 (sh, s), 1027 (s), 972 (sh, w), 889 (vw), 860 (m), 800 (m), 784 (sh, w), 752 (m), 722 (sh, vw), 701 (vw), 638 (m), 617 (vw), 599 (vw). ^{1}H NMR (CD_3CN): δ 5.30 (s, C_5H_5, 10H), 4.00 (t, J_{HP} = 5.7 Hz, OCH_3, 12H), 3.70 (t, J_{HP} = 5.6 Hz, OCH_3, 12H), 3.49 (d, J_{HP} = 12.0 Hz, OCH_3, 12H), 3.0 (br s, OH). ^{31}P NMR (CD_3CN): δ 129.5 [br t, $J_{PP} \sim$ 140 Hz, 2P], 126.2 [br d, $J_{PP} \sim$ 140 Hz, 4P]. UV–vis [λ_{max}, nm (ϵ, M^{-1} cm^{-1}), in 0.1 M H_2SO_4]: 206 (2.8×10^4), 240 (4.2×10^4), 334 (1.17×10^4), 638 (2.4×10^3). UV–vis [λ_{max}, nm (ϵ, M^{-1} cm^{-1}), in CH_2Cl_2]: 242 (4.1×10^4), 336 (1.18×10^4), 628 (2.4×10^3).

$(L_{OMe})(O)Ru^V(\mu\text{-}O)_2Ru^V(O)(L_{OMe})$ (2). Excess C_6H_5IO (0.56 g, 2.5 mmol) was added to $[H_21](CF_3SO_3)_2$ (1.12 g, 0.76 mmol) dissolved in CH_3CN (200 mL) at room temperature, and the suspension was stirred 15 min to afford a deep red solution. The solution was filtered through a medium frit. Then 40% (w/w) aqueous NEt_4OH (0.50 mL, 0.76 mmol) was slowly added, immediately giving a purple solution. The solution was reduced to an oily residue by vacuum, and the residue was extracted with C_6H_6 (200 mL). The solution was filtered and reduced to 50 mL by vacuum. A purple solid precipitated on addition of heptane (100 mL). The solid was isolated on a medium frit and washed repeatedly with 1 mL portions of CH_3CN until washings were purple rather than brown. The solid was dissolved in CH_3CN (350 mL), and the solution was reduced to 10 mL by vacuum. The purple crystals were isolated on a medium frit and washed with 1-mL portions of CH_3CN until the washings were purple. Recrystallization from CH_3CN effectively removes impurities though at a cost to the yield. The solid was dried *in vacuo* and stored under argon (0.12 g, 14%). Anal. Calcd for $C_{22}H_{46}Co_2O_{13}P_6Ru_2$ (mol wt 1168.44): C, 22.61; H, 3.97. Found: C, 22.90; H, 3.90. IR (KBr): 3123 (w), 2994 (w), 2948 (m), 2901 (m sh), 2842 (w), 1459 (m),

(10) Breiter, M. W. Electrochemical Processes in Fuel Cells. In *Anorganische und Allgemeine Chemie in Einzeldarstellungen*; Springer-Verlag: New York, 1969; Vol. 9. Archer, D. H.; *et. al.* In *Energy Conversion Systems*; Grimes, P. G., Ed.; Chemical Engineering Progress Symposium Series; American Institute of Chemical Engineers: New York, 1967. Bockris, J. O'M.; Srinivasan, S. *Fuel Cells: Their Electrochemistry*; McGraw-Hill: New York, 1969.
(11) Power, J. M.; Evertz, K.; Henling, L.; Marsh, R.; Schaefer, W. P.; Labinger, J. A.; Bercaw, J. E. *Inorg. Chem.* **1990**, *29*, 5058–5065.
(12) Kläui, W. *Angew. Chem., Int. Ed. Engl.* **1990**, *29*, 627.
(13) El-Hendawy, A. M.; Griffith, W. P.; Tahn, F. I.; Moussa, M. H. *J. Chem. Soc., Dalton Trans.* **1984**, 901. Raven, S. J.; Meyer, T. J. *Inorg. Chem.* **1988**, *27*, 4478–4483.
(14) Griffith, W. P.; Pawson, D. *J. Chem. Soc., Dalton Trans.* **1973**, 1315.
(15) Saltzman, H.; Sharefkin, J. G. *Organic Synth.* **1965**, *43*, 60–61.
(16) Kläui, W. *Z. Naturforsch., B.: Anorg. Chem., Org. Chem.* **1979**, *34B*, 1403. Griffith, W. P.; Pawson, D. *J. Chem. Soc., Dalton Trans.* **1973**, 1315.

1425 (m), 1175 (m), 1143 (m sh), 1104 (s), 1073 (s), 1032 (s), 1008 (s), 850 (s), 836 (m), 784 (m), 734 (s), 617 (s), 599 (s), 472 (m). ^{1}H NMR (CD_3CN): δ 4.937 (s, C_5H_5, 10H), 3.92 (t, J_{HP} = 4.6 Hz, OCH_3, 12H), 3.52 (t, J_{HP} = 4.6 Hz, OCH_3, 12H), 3.36 (d, J_{HP} = 10.5 Hz, OCH_3, 12H). ^{1}H NMR (CD_2Cl_2): δ 4.94 (s, C_5H_5, 10H), 3.98 (t, J_{HP} = 5.3 Hz, OCH_3, 12H), 3.58 (t, J_{HP} = 5.1 Hz, OCH_3, 12H), 3.43 (d, J_{HP} = 10.0 Hz, OCH_3, 12H). UV–vis [λ_{max}, nm (ϵ, M^{-1} cm–1), in CH_2Cl_2]: 242 (4.1 × 10^4), 332 (9.2 × 10^3), 564 (3.1 × 10^3).

[(L_{OMe})(CH_3CN)Ru^{III}(μ-OH)$_2$$Ru^{III}$($NCCH_3$)($L_{OMe}$)][$CF_3SO_3$]$_2$ ([3][CF_3SO_3]$_2$). CH_3CN (40 mL) was added to a mixture of Ph_3P (0.0557 g, 0.212 mmol) and [H_2**1**][CF_3SO_3]$_2$ (0.1498 g, 0.1019 mmol), and the solution was stirred for 18 h at room temperature, then pumped to dryness. The residue was suspended in CH_2Cl_2 (10 mL), and the yellow powder was isolated on a small medium frit. The solid was washed with CH_2Cl_2 and dried *in vacuo* (0.124 g, 0.082 mmol, 80%). Anal. Calcd for $C_{28}H_{54}Co_2F_6N_2O_{26}P_6Ru_2S_2$ (mol wt 1518.69): C, 22.14; H, 3.58; N, 1.84. Found: C, 21.95; H, 3.62; N, 1.92. IR (Nujol): 3311 (w), 3122 (vw), 3094 (vw), 1791 (vw), 1461 (s), 1426 (sh, m), 1276 (s), 1261 (s), 1224 (m), 1170 (s), 1158 (s), 1082 (s), 1031 (s), 998 (s), 917 (w), 845 (m), 791 (s), 744 (s), 635 (s), 611 (s), 595 (s), 574 (w). ^{1}H NMR (CD_3CN): δ 5.20 (s, C_5H_5, 10H), 4.06 (t, J_{HP} = 5.4 Hz, OCH_3, 12H), 3.91 (t, J_{HP} = 5.2 Hz, OCH_3, 12H), 3.17 (d, J_{HP} = 10.8 Hz, OCH_3, 12H), 2.14 (s, CH_3CN, 6H). UV–vis [λ_{max}, nm (ϵ, M^{-1} cm^{-1}), in CH_2Cl_2]: 242 (3.9 × 10^4), 344 (1.68 × 10^4).

[(L_{OMe})(H_2O)Ru^{III}(μ-OH)$_2$$Ru^{III}$($OH_2$)($L_{OMe}$)][$CF_3SO_3$]-[$CH_3C_6H_4SO_3$] ([4][$CF_3SO_3$][$CH_3C_6H_4SO_3$]). A suspension containing dimer [H_2**1**][CF_3SO_3]$_2$ (0.1067 g, 0.0726 mmol) and $CH_3C_6H_4SO_3H$ (0.1249 g, 0.725 mmol) in H_2O (5 mL) was added to Zn amalgam [prepared from a suspension of Zn (0.1016 g, 1.554 mmol) and $HgCl_2$ (0.0222 g, 0.0818 mmol) in H_2O]. This suspension was agitated at room temperature until the solution changed from green to yellow and then to orange. The solution was filtered in air (whereupon the color returned to yellow) and extracted with 5 mL of CH_2Cl_2. The CH_2Cl_2 solution was dried with $MgSO_4$ and filtered. A yellow solid was precipitated by the addition of heptane (5 mL) followed by reduction to 5 mL by vacuum. The yellow powder was isolated on a small medium frit and washed with heptane and petroleum ether. The solid was dried *in vacuo* (0.0205 g, 0.0137 mmol, 18.9%). Anal. Calcd for $C_{30}H_{59}Co_2F_3O_{28}P_6Ru_2S_2$ (mol wt 1494.74): C, 24.11; H, 3.98. Found: C, 23.89; H, 4.00. IR (KBr): 3186 (m), 3118 (sh, m), 3006 (sh, w), 2954 (m), 2848 (w), 1458 (m), 1425 (w), 1281 (w), 1258 (w), 1231 (m), 1176 (m), 1124 (m), 1062 (s), 1034 (s), 1012 (sh, s), 998 (sh, s), 847 (m), 819 (w), 790 (m), 773 (sh, w), 741 (m), 712 (w), 682 (m), 651 (sh, m), 639 (m), 612 (sh, m), 598 (m), 566 (m), 455 (w). ^{1}H NMR (CD_2Cl_2): δ 7.62 (d, J_{HH} = 7.7 Hz, $CH_3C_6H_4SO_3$, 2H), 7.13 (d, J_{HH} = 7.7 Hz, $CH_3C_6H_4SO_3$, 2H), 5.15 (s, C_5H_5, 10H), 4.16 (t, J_{HP} = 5.6 Hz, OCH_3, 12H), 4.03 (t, J_{HP} = 5.6 Hz, OCH_3, 12H), 2.96 (d, J_{HP} = 11.2 Hz, OCH_3, 12H), 2.34 (s, $CH_3C_6H_4SO_3$, 3H), 1.56 (br s, O*H*). ^{1}H NMR (pH = 7 D_2O): δ 7.49 (d, J_{HH} = 8.1 Hz, $CH_3C_6H_4SO_3$, 2H), 7.17 (d, J_{HH} = 8.1 Hz, $CH_3C_6H_4SO_3$, 2H), 5.32 (s, C_5H_5, 10H), 3.97 (q, J_{HP} = 3.6 Hz, OCH_3, 12H), 3.87 (q, J_{HP} = 3.6 Hz, OCH_3, 12H), 2.94 (m, J_{HP}=3.7 Hz, OCH_3, 12H), 2.20 (s, $CH_3C_6H_4SO_3$, 3H). UV–vis [λ_{max}, nm (ϵ, M^{-1} cm^{-1}), in CH_2Cl_2]: 242 (4.2 × 10^4), 342 (1.58 × 10^4).

[(L_{OMe})(H_2O)Ru^{III}(μ-OH)(μ-OH_2)Ru^{III}(OH_2)(L_{OMe})][CF_3SO_3]$_3$ ([H4][CF_3SO_3]$_3$). A solution of [H_2**1**][CF_3SO_3]$_2$ (0.1020 g, 0.0694 mmol), NaH_2PO_4·H_2O (0.899 g, 6.51 mmol), and H_3PO_4 (85% w/w) (0.21 mL, 3.07 mmol), dissolved in H_2O (65 mL) was electrolyzed at 0.15 V versus SCE (2.0 C of charge) at a Pt-gauze electrode in a two-compartment electrochemical cell with stirring. An excess of $NaCF_3SO_3$ (0.42 g, 2.44 mmol) was added, causing a yellow solid to precipitate. The solid was collected on a medium frit and dissolved in CH_2Cl_2 (50 mL) under argon. The solution was filtered, and its volume was reduced by vacuum until solid began to appear. Heptane (30 mL) was added and the solution volume was further reduced by vacuum until the solution was colorless. The yellow powder was isolated on a small medium frit and washed with heptane and dried *in vacuo*. The pad of solid was then washed with 1-mL portions of CH_2Cl_2 until the washings were yellow rather than green. The remaining solid was dried *in vacuo* (0.0454 g, 0.0279 mmol, 40%). Anal. Calcd for $C_{25}H_{55}Co_2F_9O_{31}P_6Ru_2S_3$ (mol wt 1624.71): C, 18.48; H, 3.41. Found: C, 18.68; H, 3.32. IR (KBr): 3313 (br, m), 3125 (sh, m), 3007 (w), 2956 (m), 2899 (w), 2851 (w), 1793 (br, w), 1462 (m), 1427 (m), 1290 (sh, w), 1267 (s), 1226 (sh, m), 1166 (s), 1071 (s), 1029 (s), 1004 (sh, s), 944 (sh, w), 853 (m), 791 (s), 745 (s), 638 (s), 616 (s), 599 (sh, m), 576 (sh, w), 517 (w), 482 (w), 459 (w). ^{1}H NMR (D_2O, pH = 7): δ 5.33 (s, C_5H_5, 10H), 3.97 (q, J_{HP} = 3.6 Hz, OCH_3, 12H), 3.88 (q, J_{HP} = 3.6 Hz, OCH_3, 12H), 2.94 (q, J_{HP} = 3.7 Hz, OCH_3, 12H). ^{1}H NMR (CD_2Cl_2): δ 5.21 (s, C_5H_3, 10H), 4.20 (t, J_{HP} = 5.4 Hz, OCH_3, 12H), 4.04 (t, J_{HP} = 5.4 Hz, OCH_3, 12H), 3.11 (d, J_{HP} = 10.7 Hz, OCH_3, 12H), 1.55 (br s, O*H*). UV–vis [λ_{max}, nm (ϵ, M^{-1} cm^{-1}), in CH_2Cl_2]: 242 (3.9 × 10^4), 342 (1.75 × 10^4).

[(L_{OMe})Ru^{III}(μ-OH)$_2$(μ-HCOO)Ru^{III}(L_{OMe})][CF_3SO_3]·2H_2O ([5][CF_3SO_3]·2H_2O). An excess of 37% aqueous CH_2O was added to a solution of [H_2**1**][CF_3SO_3]$_2$ (0.1095 g, 0.0745 mmol), NaH_2PO_4·H_2O (0.0512 g, 0.371 mmol), and Na_2HPO_4·7H_2O (0.0595 g, 0.222 mmol) in H_2O (15 mL). This solution was heated to 80 °C with stirring until the solution became yellow (15 min). The reaction was extracted with CH_2Cl_2 (2 × 7.5 mL), and the extracts were dried with $MgSO_4$ and filtered. The product was precipitated by addition of heptane (45 mL). The yellow microcrystalline solid was isolated on a medium frit and washed sequentially with CH_2Cl_2/heptane (1:3), heptane, and petroleum ether. The solid was dried *in vacuo* (0.0739 g, 0.0499 mmol, 72.5%). Anal. Calcd for $C_{24}H_{53}Co_2F_3O_{27}P_6Ru_2S$ (mol wt 1368.57): C, 21.06; H, 3.90. Found: C, 21.07; H, 3.52. IR (KBr): 3527 (s), 3451 (s), 3172 (sh w), 3120 (m), 3001 (m), 2951 (s), 2902 (sh, m), 2845 (m), 2050 (br, w), 1774 (br, w), 1636 (w), 1570 (s), 1460 (m), 1427 (m), 1376 (w), 1348 (m), 1281 (s), 1260 (s), 1224 (m), 1174 (sh, s), 1158 (s), 1107 (sh, s), 1080 (s), 1036 (s), 1010 (vs), 875 (sh, w), 853 (m), 838 (sh, w), 789 (s), 772 (sh, s), 739 (s), 657 (sh, m), 638 (s), 614 (sh, s), 601 (s). ^{1}H NMR (D_2O, pH = 7, I = 0.1 M): δ 5.29 (s, C_5H_5, 10H), 3.86 (q, J_{HP} = 5.4 Hz, OCH_3, 24H), 3.09 (d, J_{HP} = 11.1 Hz, OCH_3, 12H). ^{1}H NMR (CD_2Cl_2): δ 12.27 (s, μ-*H*COO, 1H), 5.23 (s, C_5H_5, 10H), 4.04 (m, OCH_3, 24H), 3.21 (m, OCH_3, 12H), 1.62 (br s, O*H*). UV–vis [λ_{max}, nm (ϵ, M^{-1} cm^{-1}), in CH_2Cl_2]: 242 (3.8 × 10^4), 342 (1.46 × 10^4), 694 (8.4 × 10).

[(L_{OMe})Ru^{IV}(μ-O)$_2$(μ-HCOO)Ru^{IV}(L_{OMe})][CF_3SO_3] ([6][CF_3SO_3]). Solid $AgCF_3SO_3$ (0.0265 g, 0.103 mmol) was added to a solution of (**5**)(CF_3SO_3) (0.0506 g, 0.0344 mmol), NaH_2PO_4·H_2O (0.0480 g, 0.348 mmol), and Na_2HPO_4·7H_2O (0.0590 g, 0.220 mmol) in H_2O (15 mL). The resulting pale yellow suspension was sonicated until the suspension became a dark green (30 min). The suspension was filtered and extracted three times with 15, 10, and 5 mL of CH_2Cl_2, respectively. The combined CH_2Cl_2 solutions were dried with $MgSO_4$ and filtered. The product was precipitated by addition of heptane (120 mL) followed by reduction to 75 mL by vacuum. The green powder was isolated on a medium frit and washed with heptane and petroleum ether. The green powder was dried *in vacuo* (0.0431 g, 0.0323 mmol, 93.9%). Anal. Calcd for $C_{24}H_{47}Co_2F_3O_{25}P_6Ru_2S$ (mol wt 1330.52): C, 21.67; H, 3.56. Found: C, 21.66; H, 3.52. IR (KBr): 3591 (br, sh, m), 3116 (w), 3000 (w), 2952 (m), 2904 (sh, w), 2846 (w), 1995 (br, vw), 1790 (br, vw), 1541 (m), 1460 (m), 1427 (w), 1353 (m), 1277 (m), 1224 (m), 1174 (sh, m), 1156 (m), 1066 (sh, s), 1031 (s), 850 (w), 793 (m), 743 (m), 696 (w), 638 (m), 619 (sh, m), 604 (m), 518 (w), 496 (w). ^{1}H NMR (pH = 7, D_2O): δ 5.21 (s, C_5H_5, 10H), 3.75 (m, OCH_3, 12H), 3.48 (m, OCH_3, 12H), 3.34 (m, OCH_3, 12H). ^{1}H NMR (CD_2Cl_2): δ 5.20 (s, C_5H_3, 10H), 3.93 (pseudo t, J_{HP} = 5.6 Hz, OCH_3, 12H), 3.62 (pseudo t, J_{HP} = 5.6 Hz, OCH_3, 12H), 3.42 (d, J_{HP} = 11.1 Hz, OCH_3, 12H). UV–vis [λ_{max}, nm (ϵ, M^{-1} cm^{-1}), in CH_2Cl_2)]: 242 (4.0 × 10^4), 336 (1.21 × 10^4), 672 (1.91 × 10^3).

[(L_{OMe})Ru^{III}(μ-OH)$_2$(μ-OH_2)Ru^{III}(L_{OMe})][CF_3SO_3]$_2$ ([7][CF_3SO_3]$_2$). A solution of [H_2**1**][CF_3SO_3]$_2$ (0.1032 g, 0.0702 mmol), Na_2HPO_4·7H_2O (0.4099 g, 1.529 mmol), and Na_3PO_4·12H_2O (0.1279 g, 3.37 mmol) in H_2O (65 mL) was electrolyzed (2.0 C at –0.55 V versus SCE) at a Pt-gauze electrode in a two-compartment cell (the other compartment also contained phosphate buffer) with stirring. The resulting solution was extracted with CH_2Cl_2 (3 x 20 mL). The extractions were dried with $MgSO_4$ and filtered. The product was precipitated by addition of heptane (120 mL) followed by reduction to 100 mL by vacuum. The solid was isolated on a medium frit and washed with heptane and petroleum ether. The yellow powder was dried *in vacuo* (0.0388 g, 0.030 mmol, 42%). Anal. Calcd for $C_{24}H_{50}Co_2F_6O_{27}P_6Ru_2S_2$ (mol wt 1454.60): C, 19.82; H, 3.46. Found: C, 20.03; H, 3.56. IR (KBr): 3524 (sh, br, m), 3124 (w), 3004 (w), 2951 (m), 2901 (br, w), 2844 (w), 1439 (w), 1425 (w), 1284 (m), 1262 (m), 1253 (m), 1224 (w), 1174 (sh, m), 1157 (m), 1070 (s), 1039 (s), 1032 (s), 1009 (sh, s), 844 (w), 790 (m), 740 (m), 638 (m), 621 (m), 518 (vw), 485 (vw). ^{1}H NMR (pH = 7, D_2O): δ 5.37 (s, C_5H_5, 10H), 3.75 (m, OCH_3, 36H). UV–vis [λ_{max}, nm (ϵ, M^{-1} cm^{-1}), in CH_2Cl_2]: 244 (4.0 × 10^4), 342 (1.46 × 10^4).

[(L_{OMe})(HO)Ru^{III}(μ-OH)$_2$$Ru^{III}$($NCCH_3$)($L_{OMe}$)][$CF_3SO_3$]·$H_2O$ ([8][CF_3SO_3]·H_2O). An excess of Me_3CNH_2 (90 μL, 0.86 mmol) was added to a suspension of [H_2**1**][CF_3SO_3]$_2$ (0.2003 g, 0.1362 mmol) in CH_3CN (20 mL). The resulting yellowish green solution was quickly degassed and refluxed under an atmosphere of argon for 1 h. The orange solution was pumped to dryness by vacuum. The residue was extracted with CH_2Cl_2 (60 mL). The CH_2Cl_2 solution was then extracted with

water (10 x 30 mL). The CH_2Cl_2 solution was dried with anhydrous $MgSO_4$ and filtered. A flocculent solid precipitated upon addition of petroleum ether (400 mL). The solid was allowed to settle. The solid was isolated on a medium frit, washed with 1:4 CH_2Cl_2–petroleum ether (3 x 3 mL), and dried *in vacuo* (0.0665 g, 0.0488 mmol, 35.8%). Anal. Calcd for $C_{25}H_{54}Co_2P_6O_{25}Ru_2NF_3S$ (mol wt 1363.60): C, 22.02; H, 3.99; N, 1.03. Found: C, 21.75; H, 3.74; N, 1.08. IR (Nujol): 4328 (vw), 4257 (vw), 3616 (m), 3519 (w), 3283 (m), 3118 (w), 2677 (vw), 2615 (vw), 1786 (vw), 1626 (vw), 1571 (vw), 1549 (vw), 1428 (m), 1282 (s), 1262 (s), 1224 (m), 1176 (m), 1159 (m), 1098 (s), 1070 (s), 1036 (s), 1002 (s), 847 (m), 837 (m), 791 (s), 740 (s), 694 (m), 638 (s), 618 (s), 600 (s), 572 (w). ^1H NMR (CD_3CN): δ 5.18 (s, C_5H_5, 5H), 5.16 (s, C_5H_5, 5H), 3.86 (t, J_{HP} = 5.2 Hz, OCH_3, 6H), 3.83 (t, J_{HP} = 5.5 Hz, OCH_3, 6H), 3.61 (t, J_{HP} = 5.6 Hz, OCH_3, 6H), 3.57 (t, J_{HP} = 5.1 Hz, OCH_3, 6H), 3.46 (d, J_{HP} = 11.2 Hz, OCH_3, 6H), 3.41 (d, J_{HP} = 11.2 Hz, OCH_3, 6H), 2.30 (br s, OH), 1.98 (s, $NCCH_3$, 3H). UV–vis (λ_{max}, nm (ϵ, M^{-1} cm^{-1}), in CH_2Cl_2): 242 (3.2×10^4), 330 (1.26×10^4), 738 (1.07×10^3).

$[(L_{OMe})Ru^{III}(\mu\text{-}OH)_2(\mu\text{-}H^{13}COO)Ru^{III}(L_{OMe})][CF_3SO_3]\cdot 2H_2O$ ($(H^{13}COO)$-[5][CF_3SO_3]·2H_2O). An excess of 19% $^{13}CH_2O$(aq) (10 equiv) was added to a suspension of $[H_21][CF_3SO_3]_2$ in phosphate buffer (pH = 7, I = 0.1 M) to afford $(H^{13}COO)$-$[5]^+$, which was isolated as the $CF_3SO_3^-$ salt as described above for the synthesis of $[5]^+$. ^{13}C NMR (CD_2Cl_2, δ 53.5): δ 179.5 (d, J_{CH} = 214 Hz, μ-$H^{13}COO$). ^{13}C NMR (pH = 7 D_2O): δ 180.7 (d, J_{CH} = 217 Hz, μ-$H^{13}COO$).

$[(L_{OMe})Ru^{IV}(\mu\text{-}O)_2(\mu\text{-}H^{13}COO)Ru^{IV}(L_{OMe})][CF_3SO_3]$ ($(H^{13}COO)$-[6][CF_3SO_3]). $(H^{13}COO)$-[6][CF_3SO_3] was prepared by the reaction of excess $AgCF_3SO_3$ with $(H^{13}COO)$-[5][CF_3SO_3]·2H_2O in phosphate buffer as described above for the synthesis of [6][CF_3SO_3]. ^{13}C NMR (pH = 7 D_2O): δ 167.2 (d, J_{CH} = 167.1 Hz, μ-$H^{13}COO$).

Reaction of [6][CF_3SO_3] with $^{13}CH_2O$. An excess of $^{13}CH_2O$ (aq) (7.1 μL, 19%, 50 μmol) was added to a suspension of [6][CF_3SO_3] (7.7 mg, 5.2 μmol) and [5][CF_3SO_3]·2H_2O (promoter–see discussion, 1.9 mg, 1.3 μmol) in D_2O phosphate buffer (0.5 mL, pH = 7, I = 0.1 M). This mixture was heated to 75 °C until the reaction became a yellow-brown solution (30 min). ^{13}C NMR (pH = 7 D_2O): δ 171.3 (d, J_{CH} = 195 Hz, free $H^{13}COO^-$), 82.0 (t, J_{CH} = 164 Hz, excess free $^{13}CH_2O$).

Reaction of (μ-$H^{13}COO$)-[6][CF_3SO_3] with CH_2O. An excess of CH_2O(aq) (3.75 μL, 37%, 5.0 μmol) was added to a suspension of (μ-$H^{13}COO$)-[6][CF_3SO_3] (7.4 mg, 5.0 μmol) and (μ-$H^{13}COO$)-[5]-[CF_3SO_3]·2H_2O (2.5 mg, 1.7 μmol) in D_2O phosphate buffer (0.5 mL, pH = 7, I = 0.1 M). This mixture was heated to 75 °C until the reaction became a yellow-brown solution (30 min). ^{13}C NMR (pH = 7 D_2O): δ 180.9 (d, J_{CH} = 217 Hz, μ-$H^{13}COO$) {this signal characteristic of (μ-$H^{13}COO$)-$[5]^+$}, 171.3 trace (free $H^{13}COO^-$).

Reaction of [H4][CF_3SO_3]$_3$ with CD_3CN. [H4][CF_3SO_3]$_3$ (0.0050 g, 3.52 μmol) was suspended in CD_3CN (0.7 mL) in an NMR tube. The ^1H NMR spectrum was collected immediately, and indicated a mixture of soluble $[H4]^+$ and $[3]^{2+}$. The NMR tube was heated to 40 °C for 20 min during which time all of the suspended solid dissolved. The ^1H NMR spectrum then showed only $[3]^{2+}$.

Reactions of [H_21][CF_3SO_3]$_2$ with Substrates in CD_3CN. [H_21][CF_3SO_3]$_2$ (0.0751 g, 0.0517 mmol) was dissolved into CD_3CN (10 mL). This solution was divided into 10 1.00-mL portions. Then about 3 equiv of a substrate was added to each: $C_6H_5CH_2OH$ (1.6 μL, 15.5 μmol); CH_3CH_2OH (0.9 μL, 15.3 μmol); C_6H_5CHO (1.5 μL, 14.8 μmol); CH_3OH (0.6 μL, 14.8 μmol); cyclohexene (1.5 μL, 14.8 μmol); $(CH_3)_2CHOH$ (1.2 μL, 15.7 μmol); CH_3COOH (0.9 μL, 15.7 μmol); C_6H_5COOH (0.0018 g, 14.7 μmol); $C_5H_5NH_2$ (1.4 μL, 15.4 μmol); 2,6-$(CH_3)_2C_6H_3NH_2$ (0.0018 g, 14.9 μmol). Liquids were added by microsyringe. These solutions were heated in closed vials at 76 °C for an hour. The solutions were transferred to NMR tubes, and their spectra were collected. These spectra were compared to those of authentic samples of the corresponding organic oxidation products in CD_3CN.

Crystal Structure Determination of $[(L_{OMe})(CH_3CN)Ru^{III}(\mu\text{-}OH)_2Ru^{III}(NCCH_3)(L_{OMe})][CF_3SO_3]_2$ ([3][CF_3SO_3]$_2$). X-ray quality crystals were grown by room temperature vapor diffusion of petroleum ether into a CH_2Cl_2 solution of the dimer. A yellow tabular crystal (0.3 mm x 0.4 mm x 0.7 mm) was mounted on a glass fiber with epoxy. A data set of 9449 reflections was collected at 298 K on an Enraf-Nonius Cad-4 diffractometer over the range $2° < 2\theta < 50°$ over all of the $\pm h$, $\pm k$, $\pm l$ octants by an ω-scan method. These data were merged with a goodness of fit of 1.02 to give 4669 independent reflections. General crystallographic data are listed in Table I. Computations were done with the CRYM crystallographic computing system[17] and the drawings were made with ORTEP.[18] Published values were used for the scattering factors f_o and f'.[19] No corrections for extinction were made. The Ru, Co, and P atoms were located from a Patterson map and the remaining non-hydrogen atoms were located in successive structure factor-Fourier calculations. The atom positions and temperature factors were then refined by least-squares methods, minimizing $\Sigma w(F_o^2 - F_c^2)^2$, where $w = 1/\sigma^2(F_o^2)$. The H atoms were then placed either in calculated positions (for the Cp rings) or in idealized positions based on difference maps calculated in the expected planes (for the methyl groups). The H atoms on the bridging oxygen atoms were located in a difference Fourier map. Positional and anisotropic displacement parameters of all atoms were refined in a full matrix, with the H atom thermal parameters treated isotropically. Atomic coordinates and displacement parameters are given in Table II; additional crystallographic data are available as supplementary material.

Table I. General Crystallographic Data for $[(L_{OMe})(CH_3CN)Ru^{III}(\mu\text{-}OH)_2Ru^{III}(NCCH_3)(L_{OMe})][CF_3SO_3]_2$ ([3][CF_3SO_3]$_2$) and $[(L_{OMe})Ru^{III}(\mu\text{-}OH)_2(\mu\text{-}HCOO)Ru^{III}(L_{OMe})][CF_3SO_3]\cdot 2H_2O$ ([5][CF_3SO_3]·2H_2O)

	[3][CF_3SO_3]$_2$	[5][CF_3SO_3]·2H_2O
fw	759.34[a]	1368.57
cryst syst	triclinic	monoclinic
space group	$P\bar{1}$ (#2)	$P2_1/n$ (#14)
a, Å	8.626(3)	14.356(2)
b, Å	12.275(2)	23.839(6)
c, Å	13.457(3)	15.284(3)
α, deg	71.32(2)	90.00
β, deg	85.35(2)	115.44(1)
γ, deg	80.01(3)	90.00
V, Å^3	1328.9(6)	4723.5(18)
z	2	4
T, K	298	225
D_{calcd}, g cm^{-3}	1.90	1.92
μ_{calcd}, cm^{-1}	15.46	16.42
λ(Mo Kα), Å	0.71073 with graphite monochromator	
$R(F_o)$ [reflcns with $F_o^2 > 0$]	0.040 [4451]	0.033 [7044]
$R(F_o)$ [reflcns with $F_o^2 > 3\sigma(F_o^2)$]	0.031 [3731]	0.027 [6256]
$R_w(F_o^2)$ [all reflcns]	0.004 [4669]	0.004 [7402]
$R_w(F_o^2)$ [reflcns with $F_o^2 > 3\sigma(F_o^2)$]	0.004 [3731]	0.003 [6256]
goodness of fit (S)	1.57 [4669 data, 416 params]	1.72 [7402 data, 790 params]

[a] Molecular weight of one asymmetric unit. Dimer consits of two asymmetric units.

Crystal Structure Determination of $[(L_{OMe})Ru^{III}(\mu\text{-}OH)_2(\mu\text{-}HCOO)Ru^{III}(L_{OMe})][CF_3SO_3]\cdot 2H_2O$ ([5][CF_3SO_3]·2H_2O). X-ray quality crystals were grown by the slow cooling of a CH_2Cl_2/toluene/heptane (1:2:4 respectively) dimer solution. A yellow-green wedge-shaped lozenge crystal (0.12 mm × 0.29 mm × 0.32 mm) was mounted on a glass fiber with epoxy. The monoclinic lattice parameters were determined by least-squares fit of 25 accurately centered reflections with $22° < 2\theta < 30°$. A data set of 15 660 reflections was collected at 225 °K on an Enraf-Nonius Cad-4 diffractometer over the range $2° < 2\theta < 48°$ over the octants $\pm h$, $\pm k$, $+l$ by an ω-scan method. Absorption corrections were made analytically by Gaussian integrations using the program CRYM.[17] The 15 660 reflections measured were merged to give 7402 independent reflections with a goodness of fit of 0.96 for the 7204 multiple reflections. General crystallographic data are given in Table I. This structure was solved using the same programs and structure factors referenced above. The Ru positions were determined from a Patterson map and the remaining non-H atoms were located from repeated structure factor–Fourier cycles. The H atoms were located at peaks in a difference map in calculated planes. All atoms were refined with the H atom thermal parameters

(17) Duchamp, D. J. Presented at the American Crystallographic Association Meeting, Bozeman, MT, 1964; Paper B14, pp 29–30.
(18) Johnson, C. K. *ORTEPII. Report ORNL-3794*; Oak Ridge National Laboratory: Oak Ridge, TN, 1976.
(19) Cromer, D. T.; Waber, J. T. *International Tables for X-ray Crystallography*, **1974**, Vol. IV, Kynoch Press: Birmingham, pp 99–101, 149–151. (Present distributor: Kluwer Academic Publishers, Dordrecht, The Netherlands).

Table II. Positional and Isotropic Thermal Parameters of $[3][CF_3SO_3]_2$ (x, y, z, and $U_{eq} \times 10^4$)

atom	x	y	z	U_{eq}
Ru1	4726(0.3)	1121(0.2)	4504(0.2)	218(1)
Co1	2671(0.6)	3505(0.4)	2071(0.4)	333(1)
P1	2597(1)	1652(1)	2500(1)	297(2)
P2	2152(1)	3444(1)	3677(1)	316(2)
P3	5181(1)	3116(1)	2313(1)	298(2)
S1	1824(2)	1959(1)	7545(1)	574(3)
F1	1887(5)	489(4)	9427(3)	1162(14)
F2	−232(5)	790(5)	8710(3)	1332(16)
F3	407(6)	2056(4)	9305(3)	1431(16)
O1	2418(5)	983(3)	7207(3)	746(11)
O2	549(6)	2736(4)	6999(4)	1276(18)
O3	3004(6)	2460(5)	7816(5)	1516(20)
O4	3751(3)	816(2)	3294(2)	273(6)
O5	842(3)	1494(2)	2908(2)	432(8)
O6	2720(4)	1154(3)	1546(2)	503(8)
O7	2598(4)	4583(2)	3825(2)	459(8)
O8	319(3)	3576(2)	3965(2)	471(8)
O9	2921(3)	2403(2)	4537(2)	356(7)
O10	5939(3)	2559(3)	1439(2)	430(8)
O11	6064(4)	4220(2)	2007(2)	473(8)
O12	5779(3)	2361(2)	3393(2)	311(6)
O13	3389(3)	71(2)	5546(2)	270(7)
N1	5666(4)	1554(3)	5616(2)	292(8)
C1	930(7)	1307(6)	8819(4)	688(16)
C2	523(7)	4269(5)	1402(5)	635(17)
C3	2587(9)	5185(6)	1049(6)	846(23)
C4	1463(11)	3830(5)	712(5)	808(22)
C5	2805(8)	4384(8)	486(5)	911(28)
C6	1187(8)	5093(5)	1584(5)	692(19)
C7	6069(5)	1886(4)	6223(3)	356(10)
C8	6601(7)	2286(7)	7029(5)	689(17)
C9	454(6)	340(5)	3437(5)	579(15)
C10	4146(8)	660(7)	1149(5)	719(17)
C11	2533(12)	4688(6)	4852(6)	874(22)
C12	−408(7)	2623(6)	4640(6)	712(18)
C13	7576(6)	2079(6)	1417(5)	639(17)
C14	6259(9)	4808(6)	2723(6)	728(18)
H27	3308(46)	266(33)	5985(29)	1.7(10)[b]

[a] $U_{eq} = {}^1/_3\sum_i\sum_j[U_{ij}(a_i^*a_j^*)(\tilde{a}_i\cdot\tilde{a}_j)]$, in Å^2. [b] Isotropic displacement parameter, B, Å^2.

treated isotropically (except those on water molecule 1, which were fixed at peaks in a difference map). Least-squares refinement was as for $[3][CF_3SO_3]_2$ performed on F^2, $w = 1/\sigma^2(F_o^2)$, using one full matrix. Atomic coordinates and displacement parameters are given in Table III.

Electrochemical Measurements. Electrochemical measurements were made with the BAS 100A Electrochemical Analyzer using one- and two-compartment sample cells. All experiments were performed under inert (Ar) atmospheres in aqueous phosphate, pyrophosphate, borate, and acetate buffers. Cyclic voltammetry was carried out on disk electrodes of gold, platinum, glassy carbon, basal-plane graphite, and edge-plane graphite. The best results (free from adsorption waves) were obtained with electrodes of edge-plane graphite. Chronoamperometric measurements were made using edge-plane graphite electrodes. Rotating disk electrode experiments were made using glassy-carbon rotating disk electrodes. Bulk electrolysis measurements were made with sheets of platinum gauze as working electrodes. A Ag/AgCl (3 M NaCl) reference electrode was used in the RDE experiments (the potentials being corrected to values versus SCE), and a SCE reference electrode was used in all other experiments.

General potential measurements, assessments of reversibility, and approximate pH dependence measurements were made by cyclic voltammetry. Further potential versus pH measurements were made by RDE measurements during titrations of buffers prepared with acetic, phosphoric, and boric acids. Coulometry during bulk electrolysis was used to determine n_{eff} for redox processes with and without substrates. Chronoamperometry was used to examine the kinetics of the electrooxidation of methanol catalyzed by the dimer (**1**). Currents were sampled at times (1, 2, and 3 s) where the dimer was confirmed to exhibit good Cottrell behavior. Catalytic rates were calculated by standard methods assuming a simple catalytic cycle.[20] These rates were measured with varying catalyst and substrate concentrations and varying buffer pH's and ionic strengths. Isotope effects were examined by the use of deuterated substrates (CD_3OD).

Kinetic Measurements on Oxidation of Formaldehyde by 1. The disappearance of **1** was followed by the decay of the 680-nm peak in the UV–vis spectrum. Concentration versus time curves were obtained for ranges of dimer and substrate concentrations, buffer ionic strengths, buffer pH's, and temperatures. Isotope effects were probed by the use of D_2O buffers and CD_2O.

Table III. Positional and Isotropic Thermal Parameters of $[5][CF_3SO_3]\cdot 2H_2O$ (x, y, z and $U_{eq}{}^a \times 10^4$)

atom	x	y	z	U_{eq}
RuA	8187(0.2)	1478(0.1)	8675(0.2)	135(1)
RuB	9706(0.2)	1069(0.1)	8444(0.2)	137(1)
O1A	6805(2)	1195(1)	8562(2)	200(6)
O2A	7408(2)	1882(1)	7351(2)	204(6)
O3A	7952(2)	2172(1)	9349(2)	192(6)
O4A	9547(2)	1816(1)	8934(2)	194(6)
O5A	8838(2)	1094(1)	10008(2)	215(6)
O1B	11194(2)	1298(1)	8793(2)	212(6)
O2B	9282(2)	1399(1)	7071(2)	214(6)
O3B	10131(2)	299(1)	8137(2)	196(5)
O4B	8272(2)	782(1)	7989(2)	182(6)
O5B	10180(2)	731(1)	9808(2)	199(6)
C12	9636(3)	805(2)	10264(3)	217(9)
CoA	5614(0.3)	2357(0.2)	7847(0.3)	189(1)
CoB	11122(0.3)	800(0.2)	6806(0.3)	175(1)
P1A	5744(0.7)	1451(0.4)	7994(0.7)	198(2)
P2A	6560(0.7)	2316(0.4)	7055(0.7)	196(2)
P3A	6997(0.7)	2521(0.4)	9145(0.7)	190(2)
P1B	11813(0.7)	1204(0.4)	8211(0.7)	192(2)
P2B	9726(0.7)	1293(0.4)	6351(0.6)	184(2)
P3B	10403(0.7)	156(0.4)	7303(0.7)	210(2)
C1A	4027(3)	2315(2)	7084(4)	356(15)
C2A	4387(3)	2763(2)	6727(3)	360(11)
C3A	4883(3)	3138(2)	7498(4)	371(14)
C4A	4815(3)	2921(2)	8318(4)	362(12)
C5A	4290(3)	2413(2)	8066(4)	353(11)
C1B	11743(3)	1192(2)	5970(3)	259(8)
C2B	10992(3)	799(2)	5404(3)	262(9)
C3B	11306(3)	268(2)	5819(3)	285(9)
C4B	12260(3)	327(2)	6640(3)	294(9)
C5B	12531(3)	894(2)	6727(3)	291(10)
O6A	5052(2)	1232(1)	8509(2)	270(6)
O7A	5197(2)	1160(1)	6965(2)	329(7)
O8A	5807(2)	2229(1)	5947(2)	326(7)
O9A	7174(2)	2878(1)	7066(2)	347(7)
O10A	7263(2)	3166(1)	9145(2)	313(7)
O11A	6826(2)	2507(1)	10117(2)	283(6)
O6B	12811(2)	850(1)	8856(2)	308(7)
O7B	12345(2)	1793(1)	8203(2)	298(6)
O8B	8821(2)	1060(1)	5380(2)	322(7)
O9B	9956(2)	1879(1)	5973(2)	287(6)
O10B	9390(2)	−52(1)	6410(2)	357(6)
O11B	11009(2)	−423(1)	7590(2)	409(7)
C6A	5131(5)	639(2)	8763(5)	445(13)
C7A	5697(4)	820(3)	6518(4)	446(13)
C8A	6228(5)	2173(3)	5245(4)	516(18)
C9A	6690(6)	3385(3)	6559(6)	668(19)
C10A	8298(4)	3381(2)	9585(5)	430(14)
C11A	6728(4)	1977(2)	10515(4)	431(13)
C6B	13399(5)	1000(4)	9861(4)	617(20)
C7B	11792(4)	2306(2)	8058(5)	429(13)
C8B	7823(4)	895(3)	5297(4)	434(14)
C9B	9146(4)	2291(2)	5580(4)	419(13)
C10B	8637(4)	−390(3)	6559(4)	468(13)
C11B	11922(5)	−479(3)	8473(6)	653(18)
W1	9329(2)	2714(1)	7810(3)	571(9)
W2	8013(3)	−170(2)	8821(4)	638(14)
S1X	5043(0.9)	766(0.5)	2871(0.9)	473(3)
O1X	4060(2)	648(2)	2119(2)	646(11)
O2X	5080(3)	1200(2)	3525(3)	777(11)
O3X	5667(3)	288(1)	3345(3)	603(10)
CX	5760(3)	1068(2)	2255(3)	203(10)
F1X	5788(2)	691(1)	1586(2)	739(9)
F2X	5303(3)	1517(1)	1753(2)	762(9)
F3X	6716(2)	1192(2)	2846(3)	941(12)

[a] $U_{eq} = {}^1/_3\sum_i\sum_j[U_{ij}(a_i^*a_j^*)(\tilde{a}_i\cdot\tilde{a}_j)]$.

(20) Bard, A. J.; Faulkner, L. R. *Electrochemical Methods Fundamentals and Applications*; John Wiley & Sons: New York, 1980; pp 455–461.

Scheme I

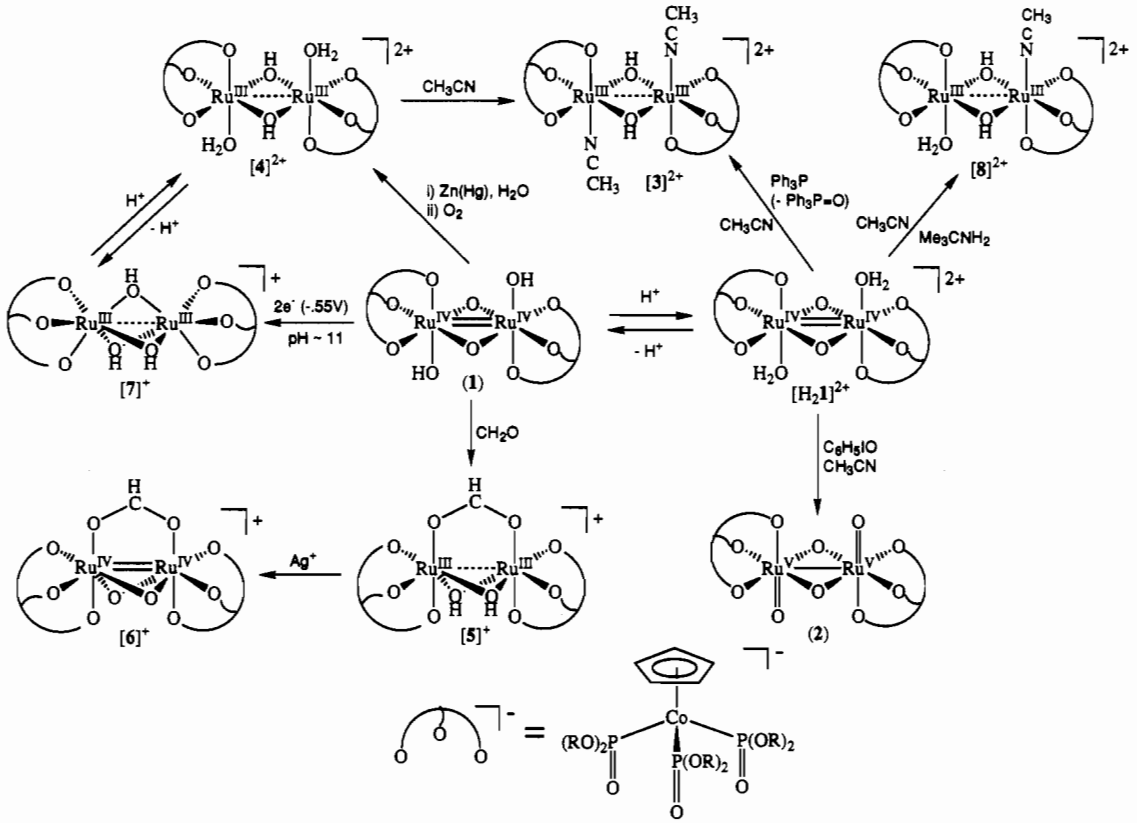

Binding of 1 in Nafion. An edge plane graphite electrode was dipped into a solution of Nafion [0.52% prepared from dilution of 5% Nafion solution (Aldrich) with 2-propanol]. After drying, the electrode was soaked either in a 0.80 mM solution of **1** or $[H_21][CF_3SO_3]_2$ in nanopure water for several hours (overnight). The electrochemistry of the electrode coating was examined in a one-compartment cell with either 0.025 M Na_2SO_4 or 0.10 M $HClO_4$ electrolyte and a SCE reference electrode. Cyclic voltammetry of electrode coatings loaded in solutions of **1** and $[H_21][CF_3SO_3]_2$ were nearly identical except for the larger currents for the former. This may be due to the added acid-base driving force for binding of **1**.

Results and Discussion

Synthesis and Electrochemistry of Complexes. Syntheses and interconversions of the various complexes that have been characterized are summarized in Scheme I. The synthetic entry to the system is via the Ru^{IV}–Ru^{IV} dimer, $[(L_{OMe})(HO)Ru^{IV}(\mu\text{-}O)_2Ru^{IV}(OH)(L_{OMe})]$ (**1**) where $(L_{OMe})^- = \{(\eta^5\text{-}C_5H_5)\text{-}Co[P(=O)(OMe)_2]_3\}^-$. The preparations of this complex and its derivatives closely follow those previously reported for the L_{OEt} analog,[11] with slight modifications due to differences in solubility attributed to the smaller alkoxy groups: L_{OMe} complexes tend to be somewhat more soluble in water and less soluble in organic solvents. As before, **1** can be diprotonated to $[(L_{OMe})(H_2O)Ru^{IV}(\mu\text{-}O)_2Ru^{IV}(OH_2)(L_{OMe})]^{2+}$ ($[H_21]^{2+}$), which reacts with excess iodosobenzene in acetonitrile followed by an equivalent of base to give the Ru^V–Ru^V dimer $[(L_{OMe})(O)Ru^V(\mu\text{-}O)_2\text{-}Ru^V(O)(L_{OMe})]$ (**2**). The two Ru^{IV}–Ru^{IV} dimers are both air stable in solution and as solids, though **1** slowly decomposes in the solid state. Storage of the Ru^{IV}–Ru^{IV} dimers as the $[H_21](CF_3SO_3)_2$ salt is preferable. The Ru^V–Ru^V dimer is water sensitive and will convert to **1** upon reaction with water in the air.[21] Under an inert atmosphere, this dimer appears stable in solution and in the solid state.

(21) We have been unable thus far to ascertain the oxidation products that accompany reduction of **2** to **1**.

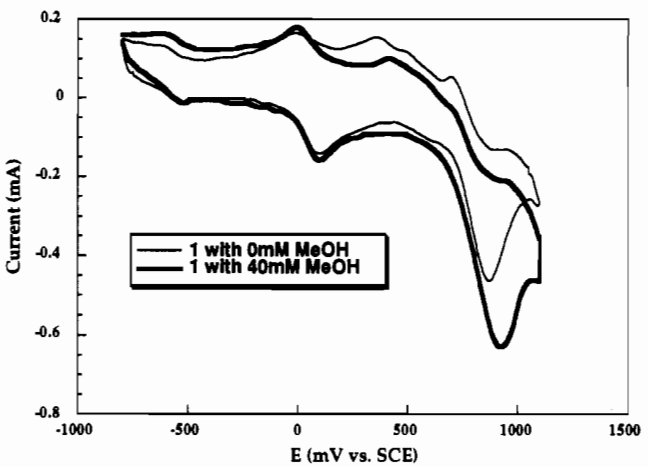

Figure 1. Cyclic voltammogram of **1** in pH 6.9 phosphate buffer with and without added CH_3OH substrate.

The ^1H NMR parameters (see Experimental Section) for **1**, $[H_21]^{2+}$, and **2** are similar in all respects to the C_s-symmetric L_{OEt} analogs (all of which were crystallographically characterized[11]) except for the replacement of ethyl by methyl signals. The use of NMR splitting patterns to determine the symmetry of these dimers was discussed previously.[11] The cyclic voltammogram of **1** is shown in Figure 1. In pH 7 phosphate buffer, **1** exhibits one oxidation (0.75 V versus SCE) and two reduction waves (0.10 V and –0.60 V versus SCE). The first reduction wave is reversible, and by bulk electrolysis is a two electron wave ($n = 1.95$), thus corresponding to a Ru^{IV}–Ru^{IV}/Ru^{III}–Ru^{III} couple. The oxidation wave and the second reduction wave are both partially to completely irreversible. At fast scan rates in acidic electrolytes, their peak currents are comparable to that of the Ru^{IV}–Ru^{IV}/Ru^{III}–Ru^{III} couple suggesting both are two-electron waves, being Ru^V–Ru^V/Ru^{IV}–Ru^{IV} and Ru^{III}–Ru^{III}/Ru^{II}–Ru^{II} couples respectively.

Ru^{III}–Ru^{III} dimers are obtained by reduction of **1**. Reaction

with Zn amalgam in water apparently leads to overreduction: prolonged stirring leads to an orange solution, which reverts to yellow on exposure to air. The moderately air-sensitive yellow $[4][CF_3SO_3][CH_3C_6H_4SO_3]$ may be isolated from this solution. In contrast, bulk electrolysis at 0.15 V versus SCE at pH = 2.5 leads directly to the Ru^{III}–Ru^{III} oxidation state; the yellow complex is isolated in its protonated form, $[H4][CF_3SO_3]_3$. Electrolysis of **1** at –0.55 V in pH ~ 11 H_2O still gives two electrons per dimer reduction and a air-stable yellow product, but the NMR is quite different from that of $[4]^{2+}$. In particular, the splitting pattern clearly shows that the molecule possesses C_3 symmetry, requiring either three identical (bridging or nonbridging) ligands or rapid exchange of protons (and deuterons) between these ligands and the D_2O solvent. The analytical data are consistent with formulation as $[(L_{OMe})Ru^{III}(\mu\text{-}OH)_2(\mu\text{-}OH_2)Ru^{III}(L_{OMe})][CF_3SO_3]_2$ ($[7][CF_3SO_3]_2$). Aqueous solutions of $[4]^{2+}$ and $[7]^{2+}$ are interconverted by changing the pH, although the reaction is slow in either direction over the range 2.5 < pH < 7.0.

The pH dependencies of the potentials of the various redox couples are shown in Figure 2. At pH = 7, **1** is neutral and $[4]^{2+}$ is a dication; the pH independence of the Ru^{III}–Ru^{III}/Ru^{II}–Ru^{II} redox potential at 3.5 < pH < 8.5 indicates that no protons are transferred, implying that the Ru^{II}–Ru^{II} species is neutral. It appears to be too reactive and/or unstable to be isolated from aqueous buffers. Similarly, the Ru^{V}–Ru^{V} dimer is not sufficiently stable in aqueous solution to isolate or completely characterize, but purple solutions of **2** in organic solvents change to red on exposure to acids such as CF_3SO_3H or upon addition to pH = 7 H_2O, suggesting that the Ru^{V}–Ru^{V} species in pH = 7 H_2O is protonated. The pH independence of the Ru^{V}–Ru^{V}/Ru^{IV}–Ru^{IV} redox potential at pH > 5.5 is not indicative of protonation state since the redox wave is totally irreversible. Below pH 5.5, where **1** is believed to be monoprotonated, the slope for the Ru^{V}–Ru^{V}/Ru^{IV}–Ru^{IV} couple is characteristic of a $2H^+$, $2e^-$ process, suggesting the Ru^{V}–Ru^{V} species is monoprotonated as well. These results suggest that at pH = 7 the redox processes are best described by eqs 1–3.

$$\underset{[H2]^+}{[(L_{OMe})(O)Ru^{V}(\mu\text{-}O)_2Ru^{V}(OH)(L_{OMe})]^+} + 2e^- + H^+ \rightleftarrows \underset{\mathbf{1}}{[(L_{OMe})(HO)Ru^{IV}(\mu\text{-}O)_2Ru^{IV}(OH)(L_{OMe})]} \quad (1)$$

$$\underset{\mathbf{1}}{[(L_{OMe})(HO)Ru^{IV}(\mu\text{-}O)_2Ru^{IV}(OH)(L_{OMe})]} + 2e^- + 4H^+ \rightleftarrows \underset{[4]^{2+}}{[(L_{OMe})(H_2O)Ru^{III}(\mu\text{-}OH)_2Ru^{III}(OH_2)(L_{OMe})]^{2+}} \quad (2)$$

$$\underset{[4]^{2+}}{[(L_{OMe})(H_2O)Ru^{III}(\mu\text{-}OH)_2Ru^{III}(OH_2)(L_{OMe})]^{2+}} + 2e^- \rightleftarrows [(L_{OMe})(H_2O)Ru^{II}(\mu\text{-}OH)_2Ru^{II}(OH_2)(L_{OMe})] \quad (3)$$

Oxidation of Organic Substrates. In organic solvents, the Ru^{V}–Ru^{V} dimer **2** readily oxidizes alcohols such as methanol, 2-propanol or *sec*-phenethyl alcohol, to give **1** and the corresponding aldehyde or ketone (eq 4). Aldehydes undergo further oxidation to the carboxylic acid (eq 8). The reactions may be followed readily by visible spectroscopy, but the kinetics are not straightforward, owing in part to the fact that **1** reacts with the same substrates (see below).[22]

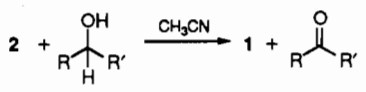

(4)

R = R' = H, CH_3; R = CH_3, R' = C_6H_5

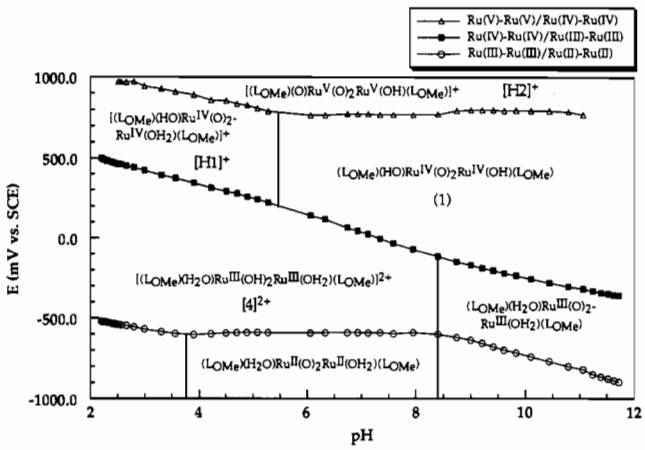

Figure 2. pH dependence of redox potentials of **1**.

The Ru^{IV}–Ru^{IV} dimer **1** oxidizes a range of substrates in both organic and aqueous solutions. In acetonitrile, $[H_21][CF_3SO_3]_2$ oxidizes triphenylphosphine to the phosphine oxide (Scheme I), alcohols (methanol, ethanol, 2-propanol, and benzyl alcohol) to their corresponding aldehydes or ketones (eq 5), and aldehydes (benzaldehyde, acetaldehyde, and formaldehyde) to their corresponding acids (eq 6). It also oxidizes anilines (2,6-di-*tert*-butylaniline and aniline), olefins (cyclohexene), and organic acids (acetic and benzoic acids), but the organic products have not been identified.

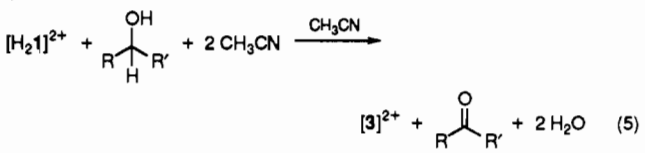

(5)

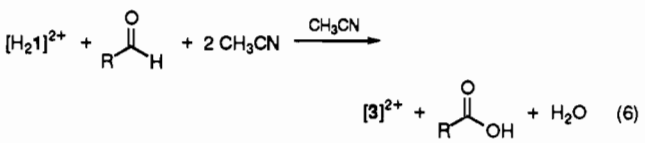

(6)

The major ruthenium product ($[3]^{2+}$) from these reactions in CH_3CN was characterized by NMR spectroscopy and X-ray crystallography as a Ru^{III}–Ru^{III} dimer, $[(L_{OMe})(CH_3CN)Ru^{III}(\mu\text{-}OH)_2Ru^{III}(NCCH_3)(L_{OMe})][CF_3SO_3]_2$ ($[3][CF_3SO_3]_2$), which is air stable in solution and in the solid state. Three other products are also obtained, in proportions depending on substrates and conditions. One of these was isolated and characterized by IR and NMR spectroscopy and elemental analysis as the asymmetric Ru^{III}–Ru^{III} dimer $[(L_{OMe})(HO)Ru^{III}(\mu\text{-}OH)_2Ru^{III}(NCCH_3)(L_{OMe})][CF_3SO_3]\cdot H_2O$ ($[8][CF_3SO_3]\cdot H_2O$). The other ruthenium products have not yet been characterized.

While the detailed mechanisms of these oxidations are not clear, it appears probable that oxidation of substrate occurs first, followed by coordination of one CH_3CN at the resulting vacancy and slower displacement of the remaining aquo ligand by CH_3CN. CH_3CN, a softer ligand than water, would be expected to coordinate preferentially to lower oxidation states. Indeed, CH_3CN does not displace the aquo ligands of **1** and $[H_21]^{2+}$, but the Ru^{III}–Ru^{III} aquo dimer $[(L_{OMe})(H_2O)Ru^{III}(\mu\text{-}OH)_2Ru^{III}(OH_2)(L_{OMe})]^{2+}$ $[4]^{2+}$ is rapidly converted to $[3]^{2+}$ in CH_3CN.

The Ru^{IV}–Ru^{IV} dimer **1** is also a good oxidant in (buffered) aqueous solution. It readily oxidizes aldehydes (benzaldehyde and formaldehyde) to the corresponding acids and, more slowly, alcohols (methanol, ethanol, and benzyl alcohol) to aldehydes and formate to carbonate. Preliminary studies of the kinetics of these reactions show complex behavior. The plot of consumption of Ru^{IV}–Ru^{IV} dimer **1** versus time (Figure 3) in the reaction with

(22) Blake, R. E.; Bercaw, J. E. Unpublished results, California Institute of Technology.

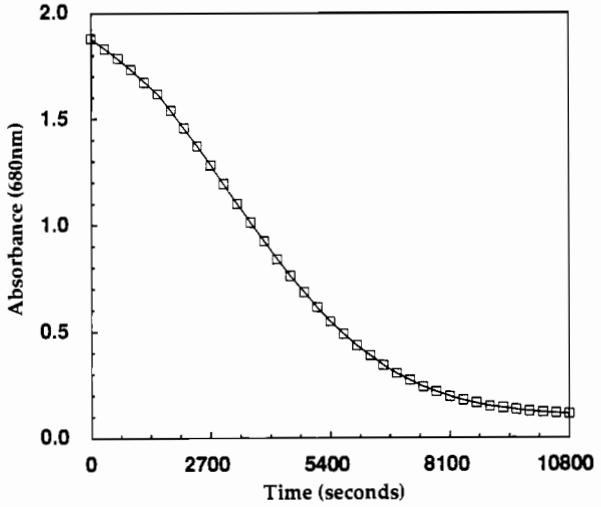

Figure 3. UV–vis absorption versus time curve for reaction of (**1**) with CH_2O. Conditions: [(**1**)] = 1.00 mM; [CH_2O] = 100 mM; 45 °C; pH = 6.9; buffer ionic strength = 0.10 M.

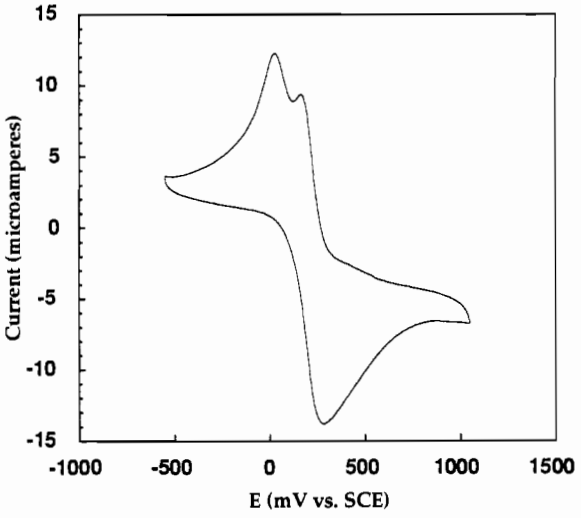

Figure 4. Cyclic voltammogram of [**5**][CF_3SO_3] in pH 6.9 phosphate buffer.

formaldehyde exhibits a small initial slope followed by acceleration, suggesting that there is an autocatalytic component. Indeed, the addition of the product Ru^{III}–Ru^{III} dimer [**5**]$^+$ (below) shortens or eliminates the initial period of slower reaction. The reaction of formaldehyde with a 1:1 mixture of **1** and [**5**]$^+$ proceeds initially at the same rate as does reaction of formaldehyde with **1** alone after 50% completion. Oxidations by **1** in organic solvents exhibit qualitatively similar behavior. More detailed kinetics studies will be reported later.

The product that results from reaction of the Ru^{IV}–Ru^{IV} dimer [H_2**1**][CF_3SO_3]$_2$ with an excess of aqueous formaldehyde is *not* the diaquo Ru^{III}–Ru^{III} dimer [**4**]$^{2+}$. NMR spectroscopy clearly shows the presence of a formate ligand; the product was isolated as an air stable yellow solid and crystallographically characterized as [(L_{OMe})Ru^{III}(μ-OH)$_2$(μ-HCO_2)Ru^{III}(L_{OMe})][CF_3SO_3]·2H_2O ([**5**][CF_3SO_3]·2H_2O). [**4**]$^{2+}$ and [**5**]$^+$ do not readily interconvert: reaction of [**4**]$^{2+}$ with excess formate does not lead to [**5**]$^+$, and no [**4**]$^{2+}$ is observed in D_2O solutions (buffered at pH 7) of [**5**]$^+$. This suggests that the oxidation of formaldehyde by **1** is an inner sphere process that leads directly to bound, not free, formate.

[**5**]$^+$ is readily oxidized. Its cyclic voltammogram shows a pseudoreversible wave at 0.20 V versus SCE at pH = 7 (Figure 4), and the formate-bridged Ru^{IV}–Ru^{IV} dimer [**6**]$^+$ may be isolated as an air stable green solid following bulk electrochemical oxidation or chemical oxidation with Ag^+. [**6**]$^+$ in turn oxidizes formaldehyde to formate. However, whereas the oxidation of formaldehyde by **1** leads essentially quantitatively to [**5**]$^+$, the yield of [**5**]$^+$ from oxidation by [**6**]$^+$ is only about 80%; additional products include the aquo and hydroxy complexes [**4**]$^{2+}$ and [**7**]$^+$. Furthermore, the oxidation by [**6**]$^+$ appears to be primarily outer-sphere. In the reaction of $^{13}CH_2O$ with unlabeled [**6**]$^+$ nearly all of the label appears as free $^{13}HCO_2^-$ (eq 7), and only a small amount of label appears in [**5**]$^+$. Conversely, if labeled [**6**]$^+$ is prepared by oxidation of labeled [**5**]$^+$ (obtained from **1** plus $^{13}CH_2O$), it reacts with unlabeled CH_2O to give labeled [**5**]$^+$ and only a trace of labeled free formate. These observations imply that a substitution-labile intermediate is formed during the outer-sphere oxidation by [**6**]$^+$, leading both to partial degradation and the small degree of isotope exchange observed.

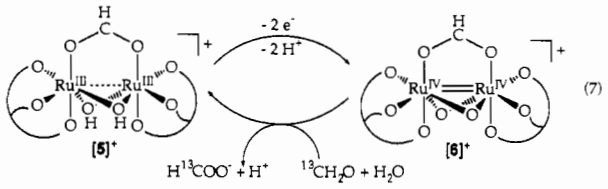

(7)

Electrocatalytic Oxidations. Although the Ru^V–Ru^V/Ru^{IV}–Ru^{IV} redox wave is not fully reversible in water, some electrocatalysis (eq 8) can be observed. The addition of alcohols (methanol, ethanol, 2-propanol, and benzyl alcohol), formaldehyde, or formate enhances the peak currents of the Ru^V–Ru^V/Ru^{IV}–Ru^{IV} couple in cyclic voltammetry (Figure 1) and results in larger currents in chronoamperometry at 0.94 V versus SCE. Preliminary kinetic results (by chronoamperometry) indicate two components to the rate law, one first order and the other zero order with respect to substrate. The latter probably involves oxidation of water and/or degradation of dimer; note in Figure 1 that new redox waves appear in the cyclic voltammogram after sweeping through the Ru^V–Ru^V/Ru^{IV}–Ru^{IV} redox wave. An isotope effect of k_H/k_D = 5 in the first-order process is measured when CD_3OH is used as substrate.

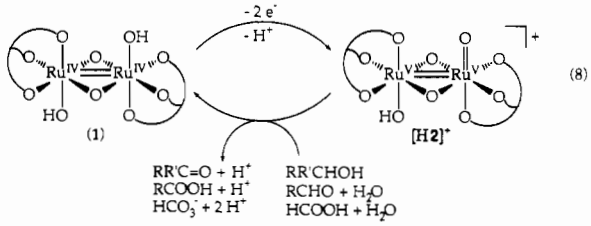

(8)

The Ru^{IV}–Ru^{IV}/Ru^{III}–Ru^{III} couple is of greater interest with respect to electrocatalysis, especially for fuel cell applications, since it is pseudoreversible, it has a low redox potential, and the Ru^{IV}–Ru^{IV} dimer **1** has been shown to oxidize substrates. The reaction of **1** with substrates such as formaldehyde is too slow on the electrochemical time scale to see definitive electrocatalysis by cyclic voltammetry or chronoamperometry even at high temperatures. However, electrocatalysis is readily demonstrated by coulometry during bulk electrooxidation of **1** and excess substrate. The total charge passed in these experiments corresponded to a number of turnovers of the catalyst dimer (Table IV). At pH 7, 86 °C, 0.10 V versus SCE, the bulk solution color changes from the green of starting **1** to the yellow of the Ru^{III}–Ru^{III} dimer, and the current gradually decays. Immediately after the solution has become yellow, cyclic voltammetry reveals a new redox wave at 0.20 V along with those of the parent compound. The color change indicates that at high temperature the reaction of **1** with formaldehyde in solution is faster than its electrochemical reoxidation at the electrode surface, and the appearance of the new wave at 0.20 V is consistent with formation of the formate-bridged Ru^{III}–Ru^{III} dimer [**5**]$^+$. Solutions electrolyzed at 0.30

Table IV. Turnover Numbers for Catalytic Oxidation of CH_2O by **1** in Phosphate Buffer

substrate	catalyst	pH	E, mV[g]	T, °C	buffer I, M[h]	n_{eff}[i]
a	*d*	2.5	500	60	0.10	5.9
a	*d*	5.5	250	71	0.10	5.1
b	*d*	6.9	300	86	0.10	25
c	*d*	8.5	–40	23	0.10	21
b	*f*	6.9	100	86	0.10	23
b	*d*	6.9	100	86	0.50	72
b	*e*	6.9	100	86	0.50	84
b	*f*	6.9	100	86	0.50	216

[a] CH_3OH (50% v/v). [b] CH_2O (108 mM). [c] CH_2O (130 mM). [d] Dimer **1** (1.0 mM). [e] 5% Pd/C ("1 mM" with respect to Pd). [f] Dimer **1** (1.0 mM) and 5% Pd/C ("1 mM" with respect to Pd). [g] In mV versus SCE. [h] Buffer ionic strength in M. [i] Effective equivalents of electrons collected; n_{eff} = 2.0 for each turnover with respect to **1**.

V also turn yellow, but subsequently return to green and then slowly become red, as the current falls to near zero.

There are (at least) two reasons why electrocatalytic oxidation does not continue indefinitely. First, as noted earlier, the product of oxidation of formaldehyde by **1** is $[5]^+$, not $[4]^{2+}$. Since $[5]^+$ is not reoxidized below 0.20 V, this would seem to suggest that no electrocatalysis should be observed at 0.10 V at all, unless some reconversion of $[5]^+$ to $[4]^{2+}$ can take place. That does not happen in solution, as shown earlier. However, the redox wave at 0.10 V remains in the cyclic voltammogram during reaction of **1** with formaldehyde and appears in voltammetry of the isolated formate complex $[5]^+$. This suggests that a small amount of $[5]^+$ may be converted to $[4]^{2+}$ during redox reactions (see above), perhaps involving a heterogeneous (substitution) reaction at the electrode, allowing the catalyst to turn over even at the low potential.

At 0.30 V electrocatalytic oxidation can proceed via the $[6]^+/[5]^+$ Ru^{IV}–Ru^{IV}/Ru^{III}–Ru^{III} couple (eq 7). Since the reaction of $[6]^+$ with formaldehyde does not proceed cleanly, however, electrocatalysis under these conditions is accompanied by gradual degradation of catalyst. This is consistent with the color changes observed; the eventual red product, which has not yet been characterized, must be incapable of participating in such a cycle.

Since this loss of activity is associated with formation of the formate complexes $[5]^+$ and $[6]^+$, it might be prevented by efficient consumption of formate. Palladium on activated carbon is known to be a good catalyst for both decomposition[23] and electrooxidation of formate;[24] when a suspension of Pd/C is added in bulk electrolysis experiments, the turnover numbers dramatically increase (Table IV). Pd/C is also a known heterogeneous electrocatalyst for the electrooxidation of CH_2O,[25] but the fact that the system with both **1** and Pd/C cocatalyst outperforms the sum of the two individual systems suggests a cooperative effect. This synergism must involve more than just consuming free formate.[26] Note that an analogous role for the platinum electrode was inferred above, to account for the catalytic turnovers observed at 0.10 V versus SCE.

The other cause for the decay in catalytic activity is the loss of pH control. In bulk electrolyses with palladium cocatalyst, the final solutions after catalyst failure are acidic (pH < 4). Oxidation of formaldehyde to formate liberates 3 equiv of acid (eq 9); when the buffer capacity of the solution has been exceeded, the pH falls and the catalyst loses activity. Both the electrochemical behavior and the stability of the ruthenium catalysts are adversely affected by acidic conditions. The number of turnovers can thus be increased simply by using a higher buffer strength (Table IV). The last entry shows that, by providing sufficient buffer *and* adding Pd/C cocatalyst, electrocatalysis can be continued for over 100 turnovers. In a fuel cell, it may in principle be possible to carry on electrocatalysis indefinitely, as the protons liberated are consumed at the oxygen cathode. Indefinite operation of an electrolytic cell should also be possible by continuously adding a compensating amount of base. Experiments to test these predictions are in progress.

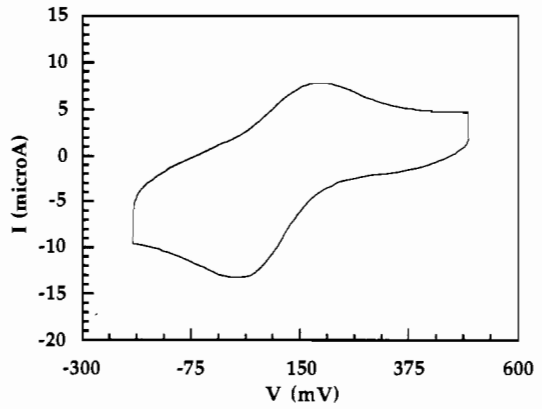

Figure 5. Cyclic voltammogram of $[H_21]^{2+}$ bound in Nafion.

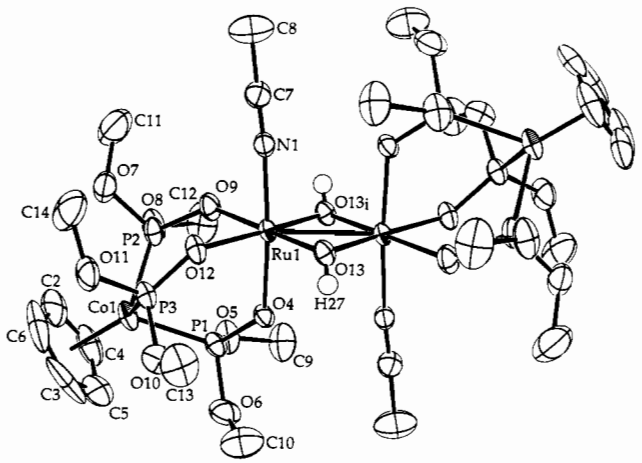

Figure 6. ORTEP of $[3]^{2+}$.

$$CH_2O + H_2O \rightarrow HCO_2^- + 3H^+ + 2e^- \qquad (9)$$

Lastly, **1** can be absorbed into Nafion films coated onto electrodes. The same cyclic voltammetric wave at around 0.10 V versus SCE is observed for the Ru^{IV}–Ru^{IV}/Ru^{III}–Ru^{III} couple as in bulk solution (Figure 5). No loss of Ru dimer from Nafion films immersed in aqueous buffers was observed even at temperatures up to 90 °C. Ru-containing Nafion-coated carbon-cloth electrodes gave larger currents for electrooxidation of formaldehyde substrate than untreated carbon cloth.

Structures of Ru^{III}–Ru^{III} Dimers. The structure of the Ru^{III}–Ru^{III} dimer $[(L_{OMe})(CH_3CN)Ru^{III}(\mu\text{-}OH)_2Ru^{III}(NCCH_3)(L_{OMe})][CF_3SO_3]_2$, $[3][CF_3SO_3]_2$, is shown in Figure 6, and selected bond lengths and angles are listed in Table V. The two halves of the edge sharing bioctahedral dimer are related by an inversion center between the two ruthenium atoms. Each ruthenium center has a pseudooctahedral environment with a facially bound L_{OMe}^- ligand (whose structural parameters are unremarkable). In contrast to the previously reported oxo-bridged structures,[11] here the ruthenium atoms are bridged by two hydroxy groups as evidenced by the longer Ru–(μ-O) distances and the easily located hydroxy hydrogen atoms (difference Fourier map).

(23) Ram, S.; Ehrenkaufer, R. E. *Synthesis* **1988**, 91 and references therein.
(24) Nishimura, K.; Yamaguti, K.; Machinda, K.-I.; Enyo, M. *J. Appl. Electrochem.* **1988**, *18*, 183–187.
(25) Manzanares, M. I.; Pavese, A. G.; Solis, V. M. *J. Electroanal. Chem.* **1991**, *310*, 159–167. Pavese, A.; Solis, V. *J. Electroanal. Chem.* **1991**, *301*, 117–127 and references therein.
(26) Perhaps an equilibrium between the diaquo Ru^{III}/Ru^{III} dimer $[4]^{2+}$ and the formate Ru^{III}/Ru^{III} dimer $[5]^+$ is involved, although this is not evident in bulk solution. Conversion of $[5]^+$ to $[4]^{2+}$ (and/or $[6]^+$ to **1**), along with consumption of the liberated formate, may be catalyzed by palladium.

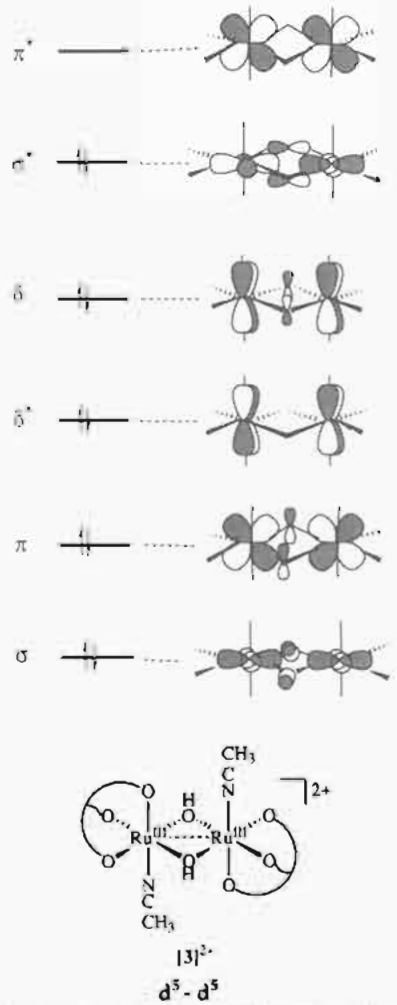

Figure 7. Qualitative molecular orbital representation of the metal–metal interaction in the edge sharing Ru^{III}–Ru^{III} complex $[3]^{2+}$ (see ref 27).

Table V. Selected Bond Lengths and Angles of $[3][CF_3SO_3]_2$

Ru–Ru$_i$	2.622 (1)	Ru–O13	2.013(3)
Ru–O4	2.054 (2)	Ru–O13$_i$	2.009 (3)
Ru–O9	2.021 (3)	Ru–N1	2.010 (3)
Ru–O12	2.044 (2)		
O4–Ru–O13	90.1 (1)	O9–Ru–N1	85.9 (1)
O4–Ru–O13$_i$	90.6 (1)	O9–Ru–O12	87.1 (1)
O4–Ru–N1	175.4 (1)	O12–Ru–O13	171.4 (1)
O4–Ru–O9	91.4 (1)	O12–Ru–O13$_i$	89.8 (1)
O4–Ru–O12	87.5 (1)	O12–Ru–N1	88.7 (1)
O9–Ru–O13	84.8 (1)	O13–Ru–O13$_i$	98.4 (1)
O9–Ru–O13$_i$	176.2 (1)	O13–Ru–N1	91.9 (1)

This bridging gives a planar $Ru_2(O)_2$ metallocycle. A terminally bound CH_3CN nitrogen occupies the remaining coordination site at each ruthenium. The Ru-Ru distance [2.622(1) Å] (Table V) is longer than that observed in the reported structures of the $(L_{OEt})^-$ analogs of **1** and $[H_21]^{2+}$, $[(L_{OEt})(H_2O)Ru^{IV}(\mu\text{-}O)_2Ru^{IV}(OH_2)(L_{OEt})](CF_3SO_3)_2$ [2.505(1) Å] and $[(L_{OEt})(HO)Ru^{IV}(\mu\text{-}O)_2Ru^{IV}(OH)(L_{OEt})]$ [2.452(1) Å].[11] This is consistent with the qualitative molecular orbital representation of the metal–metal interaction in edge sharing dimers depicted in Figure 7 which predicts a $\sigma^2\pi^2\delta^{*2}\delta^2\sigma^{*2}$ configuration for the Ru^{III}–Ru^{III} dimers and a $\sigma^2\pi^2\delta^{*2}\delta^2$ configuration for the Ru^{IV}–Ru^{IV} dimers.[27] The Ru^{III}–Ru^{III} bond distance is consistent with a net Ru–Ru single bond. It is considerably shorter than that in the Ru^{V}–Ru^{V} dimer $[(L_{OEt})(O)Ru^{V}(\mu\text{-}O)_2Ru^{V}(O)(L_{OEt})]$ [2.912(1) Å], which is considered to have no metal–metal bond at all.[11] Since $[3]^{2+}$ (like all the dimeric complexes obtained in this work) is diamagnetic, the odd spins on the two d^5 centers are paired, perhaps by superexchange through the bridging hydroxy groups or by through-space interaction.

(27) Shaik, S.; Hoffmann, R.; Fisel, C. R.; Summerville, R. H. *J. Am. Chem. Soc.* **1980**, *102*, 4555. Cotton, F. A. *Polyhedron* **1987**, *6*, 667.

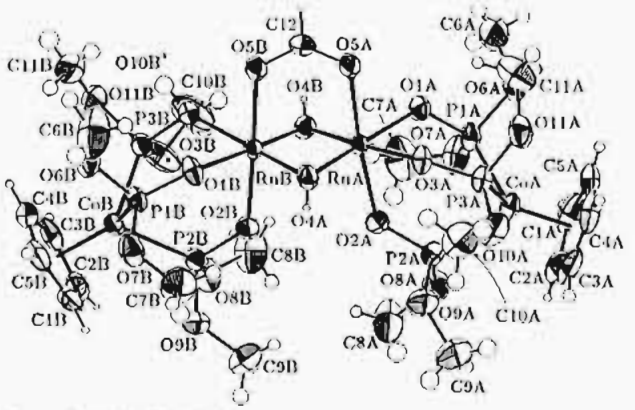

Figure 8. ORTEP of $[5]^+$.

Table VI. Selected Bond Lengths and Angles for $[5][CF_3SO_3]\cdot 2H_2O$

RuA–RuB	2.548 (1)	RuA–O4B	1.995 (3)
RuA–O1A	2.032 (2)	RuB–O4B	1.989 (3)
RuB–O1B	2.042 (2)	RuB–O4A	1.985 (3)
RuA–O2A	2.079 (2)	RuA–O5A	2.056 (2)
RuB–O2B	2.073 (2)	RuB–O5B	2.058 (2)
RuA–O3A	2.052 (2)	O5A–C12	1.247 (5)
RuB–O3B	2.051 (2)	O5B–C12	1.263 (5)
RuA–O4A	1.988 (3)		
O1A–RuA–O2A	88.5 (1)	O2B–RuB–O5B	177.8 (1)
O1B–RuB–O2B	89.0 (1)	O3A–RuA–O4A	86.1 (1)
O1A–RuA–O3A	86.8 (1)	O3B–RuB–O4B	88.7 (1)
O1B–RuB–O3B	85.3 (1)	O3A–RuA–O4B	174.3 (1)
O1A–RuA–O4A	172.3 (1)	O3B–RuB–O4A	99.8 (1)
O1B–RuB–O4B	173.1 (1)	O3A–RuA–O5A	87.9 (1)
O1A–RuA–O4B	87.5 (1)	O3B–RuB–O5B	83.1 (1)
O1B–RuB–O4A	86.5 (1)	O4A–RuA–O4B	99.6 (1)
O1A–RuA–O5A	87.0 (1)	O4B–RuB–O5A	92.7 (1)
O1B–RuB–O5B	89.2 (1)	O4A–RuA–O5A	89.6 (1)
O2A–RuA–O3A	88.8 (1)	O4B–RuB–O5B	93.6 (1)
O2B–RuB–O3B	95.4 (1)	O4B–RuA–O5A	92.7 (1)
O2A–RuA–O4A	94.5 (1)	O4A–RuB–O5B	90.6 (1)
O2B–RuB–O4B	88.1 (1)	O5A–C12–O5B	127.4 (4)
O2A–RuA–O4B	90.2 (1)	RuA–O5A–C12	121.4 (2)
O2B–RuB–O4A	90.5 (1)	RuB–O5B–C12	119.3 (2)
O2A–RuA–O5A	174.6 (1)		

The structure of the formate complex $[5]^+$ is shown in Figure 8, and selected bond lengths and angles listed in Table VI. This structure differs from those above in that the dimer is not edge sharing but face sharing, with the two ruthenium centers bridged by two hydroxy groups and a formate group. Overall, the dimer has a pseudo-C_2 axis passing through the formate ligand perpendicular to the Ru–Ru segment. Most structural parameters for the two halves correspond within experimental error. However, the Ru–O–C angles with the formate [121.4(2)°, 119.3(2)°] are significantly different, though similar. Again the ruthenium centers each have a pseudooctahedral environment with a facially coordinated L_{OMe}^- ligand (whose structural parameters are unremarkable). The hydrogen on the formate group was easily located in a difference Fourier map, and the identity of the formate group was further confirmed by undecoupled ^{13}C NMR spectroscopy of an enriched sample prepared from labeled formaldehyde. Like the Ru^{III}–Ru^{III} dimer $[3]^{2+}$ described above, the Ru–Ru distance [2.548(1) Å] is consistent with a Ru–Ru single bond and the unpaired spins on the d^5 Ru^{III} centers are paired to give overall diamagnetism. Direct comparison of the Ru–Ru distances in $[3]^{2+}$ and $[5]^+$ may not be particularly meaningful, as both the number and nature of bridging ligands differ.

Conclusions

The dimers $[(L_{OMe})(HO)Ru^{IV}(\mu\text{-}O)_2Ru^{IV}(OH)(L_{OMe})]$, $[(L_{OMe})(H_2O)Ru^{IV}(\mu\text{-}O)_2Ru^{IV}(OH_2)(L_{OMe})](CF_3SO_3)_2$, $[(L_{OMe})(O)Ru^{V}(\mu\text{-}O)_2Ru^{V}(O)(L_{OMe})]$, $[(L_{OMe})(H_2O)Ru^{III}(\mu\text{-}OH)(\mu\text{-}OH_2)Ru^{III}(OH_2)(L_{OMe})](CF_3SO_3)_3$, $[(L_{OMe})Ru^{III}(\mu\text{-}OH)_2(\mu\text{-}OH_2)Ru^{III}(L_{OMe})](CF_3SO_3)_2$, $[(L_{OMe})(CH_3CN)Ru^{III}(\mu\text{-}OH)_2Ru^{III}(NCCH_3)(L_{OMe})][CF_3SO_3]_2$, $[(L_{OMe})Ru^{III}(\mu\text{-}OH)_2(\mu\text{-}HCOO)Ru^{III}(L_{OMe})](CF_3SO_3)\cdot 2H_2O$, and $[(L_{OMe})Ru^{IV}(\mu\text{-}O)_2(\mu\text{-}HCOO)Ru^{IV}(L_{OMe})](CF_3SO_3)$ have been synthesized, and the Ru^{V}–Ru^{V} and Ru^{IV}–Ru^{IV} dimers have been shown to oxidize organic substrates. The Ru^{IV}–Ru^{IV} dimer $[(L_{OMe})(HO)Ru^{IV}(\mu\text{-}O)_2Ru^{IV}(OH)(L_{OMe})]$ is particularly intriguing in that it can function as an electrocatalyst, through its Ru^{IV}–Ru^{IV}/Ru^{III}–Ru^{III} redox couple, for oxidation of formaldehyde at low potentials (near 0.0 V versus SCE). This feature may in part be due to the oxygen-donor coordination environment and the cooperation of the ruthenium centers. Though the mechanisms for this reactivity are not yet fully understood, these systems may offer possibilities for significant advances in the design of electrocatalysts which function at low potentials useful for chemical synthesis and fuel cell technology.

Acknowledgment. This work was supported by a grant from the Office of Naval Research. E.P.K. thanks the Fanny and John Hertz Foundation for their financial support.

Supplementary Material Available: Tables giving complete positional and isotropic thermal parameters, anisotropic thermal parameters, and bond distances and angles and ORTEP drawings of $[3][CF_3SO_3]_2$ and $[5][CF_3SO_3]\cdot 2H_2O$ (31 pages). Ordering information is given on any current masthead page.